Comparison of geodetic and seismic strain rates in Greece by using a uniform processing approach to campaign GPS measurements over the interval 1994-2000

Sofia Rontogianni

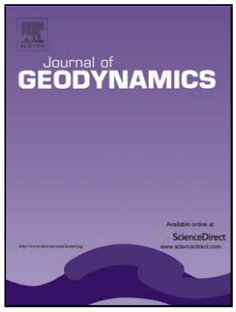

Title: Comparison of geodetic and seismic strain rates in Greece by using a uniform processing approach to campaign GPS measurements over the interval 1994-2000

Author: Sofia Rontogianni

PII: S0264-3707(10)00085-2
DOI: doi:10.1016/j.jog.2010.04.008
Reference: GEOD 1001

To appear in: *Journal of Geodynamics*

Received date: 27-7-2009
Revised date: 23-4-2010
Accepted date: 25-4-2010

Please cite this article as: Rontogianni, S., Comparison of geodetic and seismic strain rates in Greece by using a uniform processing approach to campaign GPS measurements over the interval 1994-2000, *Journal of Geodynamics* (2008), doi:10.1016/j.jog.2010.04.008

Comparison of geodetic and seismic strain rates in Greece by using a uniform processing approach to campaign GPS measurements over the interval 1994-2000

Sofia Rontogianni*

School of Civil Engineering and Geosciences, Newcastle University, NE1 7RU, UK.

*Corresponding author: Sofia Rontogianni, now at: Institute of Geophysics, National Central University, Jhongli, 320 Taiwan, E-mail: sofia@ncu.edu.tw Telephone: ++886-3-4227151 ext 65636.

Abstract

In this study we rigorously combine 18 old campaign GPS data sets from Greece covering the period 1994-2000. Although the majority of these old datasets have been analyzed and reported previously, it has not been possible to combine them into a single velocity field and apply strain analysis. Here a uniform, final coordinate solution is given by reprocessing 43 global, long-running International GNSS Service (IGS) sites together with 280 local sites. The 221 daily SINEX files are then combined in a least squares approach and the geodetic horizontal velocity field in ITRF2000 and Europe-fixed reference frame is derived. Two methods are used to compute the geodetic strain rates: (i) discrete estimates within contiguous polygons, and (ii) a continuous curvature surface fitted to the velocity field. The seismic hazard potential can be determined by comparing the geodetic and seismic strain rates. The published 300 year earthquake catalogue best describes the major active tectonic features at the scale of geodetic strain determination. The geodetic strain appears larger than the seismic strain for the majority of the region, suggesting that accumulated strain has not yet been released by earthquakes. The geodetic field is consistent with the detailed constraints implied by the observed orientations of faulting as these are given in the 300-year catalogue. We have shown that with the GPS dataset used in this work and following this processing scheme reasonable results can be obtained comparable with more recent studies, CGPS data and by recent earthquake activity.

Keywords

GPS, Greece, Velocity field, strain, seismic hazard

1. Introduction

The eastern Mediterranean is one of the most tectonically active regions on Earth as demonstrated by its seismicity and has been identified as an ideal natural laboratory for studying the kinematics and dynamics of plate interactions (McKenzie, 1978; 1972; Jackson and McKenzie, 1988; Ambraseys and Jackson, 1990; Ambraseys and Jackson, 1997; Plag et al., 1998; Ambraseys, 2001). The region is on a convergent plate boundary comprising the subduction of the African Plate under the Eurasian plate, while the Arabian plate approaches the Eurasian plate in a northwestward motion. The latter motion leads the Anatolia plate to be displaced to the west and rotate in a counterclockwise sense relative to Eurasia (Reilinger et al., 1997; McClusky et al., 2000).

In the Greek area (Figure 1) deep seismicity near Crete is related to the subduction of the northward-moving (relative to Eurasia) African oceanic lithosphere. Shallow seismicity throughout the Aegean Sea and mainland Greece is related to the southwestward (again relative to Eurasia) extension of the Aegean continental lithosphere that is driven by a combination of gravitational spreading of the Anatolian continental lithosphere from the east and roll-back of the subducting African plate to the south (Le Pichon and Angelier, 1979; Papazachos, 1990). The transition between the active lithospheric subduction and the continental collision is located around the Ionian islands (Papazachos and Kiratzi, 1996). The tectonic evolution of the Greek region has been covered in more detail elsewhere (McKenzie, 1972; 1978; Angelier et al., 1982; Armijo et al., 1996) and therefore is not elaborated upon here.

Multiple kinematic and dynamic models have been proposed as an attempt to describe the observed present-day deformation highlighting many important features of

Greece and surrounding areas (Anatolia, western Turkey), but there has not emerged a single, widely-accepted model. All agree upon N-S extension occurring within the Aegean Sea but the explanation of this differs from one study to another. In their majority they postulate that the complicated deformation observed in the Greek area is due to relative motion of a small number of rigid blocks or microplates, without agreeing upon a specific number of these, their boundaries or margins, and their rotation. It is not clear if there are zones of internal deformation in the otherwise rigid microplates that might define further microplates. Nyst and Thatcher (2004) use published site velocities from six separate GPS networks to identify deforming regions, rigid elements, and potential microplate boundaries and build upon previous work by others to initially specify rigid elements in central Greece, the southern Aegean, Anatolia and the Sea of Marmara. One main reason for quantifying the crustal deformation field lies in the constraints it can provide on the dynamics of the system. To this extent, particular focus has to be given to the role of driving forces such as gravitational collapse (e.g. western Anatolia) (Jones et al., 1996; Davies, 1997; Hatzfeld et al., 1997; Martinod et al., 2000), plate collision (e.g. the Adriatic block), push (e.g. the Arabian Plate) and slab retreat (roll-back in the Greek-Hellenic Arc). Debate still remains and various mechanical and numerical models have been published (Cianetti et al., 1997; Meijer and Wortel, 1997; Lundgren et al., 1998; Mantovani et al., 2000; Martinod et al., 2000; Cianetti et al., 2001).

The complex tectonics and high deformation rates in the Greek area have attracted in the past decade the attention of numerous scientific groups who have organized GPS campaigns and designed networks in the region. (Billiris et al., 1991; Stiros, 1993; Le

Pichon et al., 1995; Davies, 1997; Clarke et al., 1997; Reilinger et al., 1997; Clarke et al., 1998; Cocard et al., 1999; Cruddace et al., 1999; Briole et al., 2000; McClusky et al., 2000; Ayhan et al., 2002). The HELLENET and SING projects were designed to strengthen links between sites and fill in areas not previously occupied (Cruddace et al., 1999). Depending on each group's interests the locations differed as well as the network sampling interval, density and observation period at each monument. Subsequently GPS data analysis strategies also varied from campaign to campaign. Another parameter that enhanced the diversity of previous studies is that the methods and technology to measure crust deformation have improved greatly over the past two decades. This has resulted in an increased accuracy of space geodetic data derived from GPS. The improvement in accuracy in these measurements through the years is partly a direct result of the increased data volume from GPS sites, and partly the indirect result of improvements in the observational models, precise orbits and terrestrial reference frame with a continuous change and update. Because of the continuous improvement in the GPS system although the majority of these past campaign datasets have been analyzed and reported previously, it has not been possible to combine them rigorously into a single velocity field. They have been processed using different observation models (i.e. orbit types or even lack of that information in the early studies), satellite information (satellite clock correction files, satellite shadow event files, earth orientation parameters), constraints (i.e. fixed station solutions), and reference frames (ITRF94, ITRF96, ITRF97). Full variance-covariance information is not always available from previous solutions. In many cases, analysis has taken place in a regional reference frame with few or no sites overlapping other solutions, and few or no sites outside the Greek region with which to navigate the global velocity

117 solution. Efforts made to remove or make compatible existing constraints have not been
118 successful, leading each group to compute their own individual solutions.

119 This work aims 1) to reprocess 18 previous GPS campaigns, spanning from 1994-
120 2000 and including 280 local sites, combine them rigorously to obtain a unified solution
121 for the area. Our data fill gaps in potential hazardous areas such as Chalkidiki, Grevena,
122 Argos/Saronic gulfs, Egion; (2) assess how the area can be divided into zones of different
123 deformation style and rate; (3) what amount of geodetic strain is released by seismicity.
124 Strain analysis of the residual velocities to the European Euler pole is performed in order
125 to define the type of present deformation. The geodetic strain rates are estimated by two
126 methods: firstly that of contiguous uniformly-straining polygons, and secondly by
127 differentiating a minimum curvature surface fitted to the velocity field. The principal
128 horizontal strain rate tensors derived from GPS can then be compared to the seismic
129 strain rate as calculated from three earthquake catalogues covering various parts of the
130 region and spanning 30, 100 and 300 years respectively. This comparison is performed
131 for the purpose of highlighting areas of potential seismic hazard. Finally, we also
132 investigate the correspondence between the orientation of active faulting and that
133 required to accommodate the geodetic strain field.
134

135 **2. GPS data processing**

136 For the processing of the 18 campaigns (Figure 2, Table 1) we aimed to produce the best
137 possible consistency of reference frame definition, thus the frame of each campaign was
138 navigated from as many as 43 IGS (Dow et al., 2005) and EUREF (Bruyninx et al., 2001)
139 sites (Figure 3). These sites were chosen to have a global distribution and to have been in

140 continuous operation since 1994. The RINEX files for all of these stations were obtained
141 from the Scripps Orbit and Permanent Array Center (*SOPAC*)
142 http://sopac.ucsd.edu/dataArchive.

143 The raw data were imported to the software via the RINEX (Gurtner, 1994)
144 format. Where necessary, transformation from raw (in this case Trimble or Ashtech)
145 format took place using UNAVCO' s TEQC program (Estay and Meertens, 1999;
146 UNAVCO). The information given in the RINEX header was corrected in order to agree
147 with the station log files. All antenna heights were corrected to agree with the standard
148 ARP (antenna reference point) adopted by the IGS. Because the daily networks typically
149 had a mixture of antenna types, we used elevation-dependent relative phase centre offsets
150 as provided by NOAA (http://www.ngs.noaa.gov/ANTCAL).

151 For the majority of data processing we used the Bernese version 4.2 GPS
152 software, (http://www.ipa.nw.ru/PAGE/DEPFUND/GEO/nap/publ/docu42_1.pdf, Beutler
153 et al., 2001). As a reference frame for the whole solution we used ITRF2000, realized by
154 IGS precise orbits, and we applied troposphere, ionosphere, and ocean tide loading
155 corrections as described in Table 2. We corrected any detected cycle slips both
156 automatically and manually, and attempted to resolve all carrier phase ambiguities to
157 integers as part of each UT day's network solution, typically with more than 70% success
158 (Rontogianni, 2007). The three Egion campaigns were processed with the GAMIT
159 version 10.2 software using a similar strategy but with 24-hour sessions aligned to the
160 times of the local campaign observations rather than the UT day (Michael Floyd, personal
161 communication, 2007). For each campaign, the normal equations of daily sessions were
162 combined into a campaign solution as a check on processing. Daily Solution Independent

Exchange (SINEX) files were saved in order to be used in velocity analysis. For the IGS sites, the a priori velocities were given in ITRF2000 and free network conditions were set up for their coordinates.

3. Velocity field results

Blewitt and Lavallée (2002) while working with GPS data sets proposed that below 2.5 years of continuous time series, the velocity bias can become unacceptably large. They recommended that 2.5 years be adopted as a standard minimum data span for velocity solutions intended for tectonic interpretation or reference frame production. In our analysis we are working with campaign data where only the sites DION and CG54 were present in all the campaigns during the 6 years of processing and have the maximum number of observations from the local sites (Figure 4). Errors in the analysis reflect the limited number of observations, a fundamental limitation of campaign data collected by different teams, and narrow span of the time series. Site velocities have been estimated from the combination of 221 loosely-constrained daily SINEX files created by the Bernese 4.2 software, using the TANYA software developed and used at Newcastle University for IGS Global Network Associate Analysis (GNAAC) combinations (Davies, 1997; Davies and Blewitt, 2000; Lavallée, 2000). Station daily coordinates are rigorously combined using a free network approach (Davies, 1997; Davies and Blewitt, 2000). In our case the solution from Bernese 4.2 is a loosely constrained solution, and any constraints on the geometry arise from the fixed IGS orbits. The core_IGS00 SINEX file (the IGS realization of ITRF2000 Core site coordinates) was used (Altamimi et al., 2002) to navigate the solution to the ITRF2000 reference frame. Antenna height corrections and

a three dimensional data-snooping outlier rejection method are also applied if needed at this stage.

The sites were introduced in the solution starting with ones that had more than 50 daily observations (the vast majority of the IGS sites). All sites that were present in more than one campaign and had two or more daily observations were used in the final solution. A conservative limit of four standard deviations was used iteratively to exclude outliers in each station coordinate residual time series. We chose that rejection outlier boundary after considering the fact that we are dealing with small samples of campaign data and so we need to be cautious in automatically removing outliers to avoid removing data points. The resulting free network solution is aligned to ITRF2000 by applying a 12-parameter Helmert transformation (translation and rotation with their time derivatives, but no scale or scale rate). From the time series of the daily solutions we estimate a kinematic solution which for each station includes a reference epoch position at 1999.00 and a constant velocity.

For the sites whose time series were edited, no more than 10% of observations were removed. Excluded from the velocity solution are some of the IGS sites that had very noisy time series. The majority of excluded IGS sites are located in the southern hemisphere (i.e. very long baselines, with not enough overlap of visible satellites between the two stations forming the baseline). The excluded sites are YAR1, USUD, SUWN, KOKB, PIN2, KERG, HARK, and IRKT. Data for the station ANKR are used until 1999, i.e. before the devastating 1999 Izmit earthquake (17 August, Mw 7.4) that took place in this area. No other sites suffered from discernible co-seismic offsets. The output results in ITRF2000 are given in Table 3.

All errors have been scaled by the unit variance (Cross, 1992; Lavallée, 2000; Rontogianni, 2007). The sites that appear with larger velocity errors are the ones with small numbers of observations, and also sites with short time series (Figure 4). As shown in Figure 5 and Figure 6 larger velocity errors have the sites with less than 16 months data span between the first and last measurement. In this category we can place the sites from the EGION campaign. The vertical velocities are not reported since the uncertainties are too large to allow reliable interpretation.

For campaign GPS networks, scaling the errors with the unit variance leads to a very conservative error bounds. To verify that the scaling is appropriate for continuous GPS sites we also apply a chi-square test ($\chi 2/DOF$, Equation 1) to the horizontal velocity field where our velocity solution is compared with the published SOPAC solution (http://sopac.ucsd.edu/cgi-bin/refinedModelVelocities.cgi).

$$\chi^2/DOF = \frac{1}{2N}\sum_N \left(\frac{(v_E - v'_E)^2}{\sigma_E^2 + \sigma_E'^2} + \frac{(v_N - v'_N)^2}{\sigma_N^2 + \sigma_N'^2} \right) \qquad (1)$$

Where v_E, v_N and, v'_E v'_N we describe the velocities in east and north direction, for the local and SOPAC data (hyphen symbol); σ_E, σ_N and σ'_E, σ'_N are the 1-sigma errors in the two directions for both data sets; N gives the number of sites. The test value of 1.03 indicates a good agreement between the two data sets.

The ITRF2000 solution was expressed in a Europe-fixed reference frame by applying the Altamimi et al. (2002) absolute Euler pole for Eurasia (φ, °N 57.965±1.211; λ, °E -99.374±2.710; angular velocity ω, deg/Myr 0.26±0.005). As previously stated, all errors have been scaled by the unit variance; the error ellipses represent 39% confidence intervals (Table 3 and Figure 6). The sites around the Chalkidiki and Grevena area show,

231 in their majority, a very small residual motion of around 10 mm/yr. Further south there is
232 an obvious SW motion of the sites around Attica, Evia, east and south Peloponnisos as
233 well as the Aegean islands. This motion increases from ~25 mm/yr for the Aegean
234 islands to around 30 mm/yr near Attica, Evia and the eastern Peloponnisos coast, and
235 reaches ~40 mm/yr for the sites in southern Peloponnisos. The rapid displacement that is
236 concentrated in the small area of the Corinth and Patras Gulfs is very prominent. The
237 Patras area shows south-westerly motion of ~30-35 mm/yr. This kinematic field for
238 Greece has also been suggested previously e.g. Cocard et al. (1999) and Peter et al.
239 (1998) and more recently by Hollenstein et al. (2008). Hollenstein et al. while combining
240 campaign and continuous GPS data suggest that the rates increase from about 20-26
241 mm/yr in the northeastern Aegean up to 30-36 mm/yr in the southwest. They continue
242 suggesting that towards Attica the velocities reach 31.1 ± 0.1 mm/yr. There is a
243 difference in the velocity direction for the island of Astypalea probably caused by its
244 location within the eastern volcanic arc. Bohnhoff et al., 2006 after analyzing 2175
245 microseismic events in the Greek-Hellenic Volcanic Arc define the Santorini-Amorgos
246 zone as a major structural boundary of the volcanic arc subdividing it into a seismically
247 and volcanically quite western and an active eastern part. In the same study for the
248 Amorgos-Astypalea area they indicate a vertical structure possibly related to migration of
249 fluids or degassing processes SE of Amorgos.
250
251 **4. Geodetic strain analysis**
252 We use the Europe-fixed GPS velocity field to determine the crustal strain rate field and
253 rotation rates in the Greek area. We calculated the principal strain rate components using

two different methods. First we applied the polygon method which allows us to define the regions in each of which uniform strain is to be computed (e.g. based on geological criteria). The second method of deriving strain rates calculates the strain by applying continuous curvature gridding to the entire horizontal velocity dataset, and thus is independent of geological preferences and allows interpolation between points.

4.1 Polygon strain analysis

In this method the area is divided up into polygonal regions bounded by geodetic monuments. The strain rate is assumed to be spatially uniform within each polygonal region and constant with respect to time. No assumptions are made regarding the continuity of velocity or strain rate between regions (Frank, 1966; Prescott, 1976; Welsch, 1983). The choice of polygons is very important, but somewhat arbitrary although reasonable criteria can be adopted (Rontogianni, 2007). The area is quite complicated because it contains many active faults, most of which appear to have segments of around 15-20 km in length. Primarily we created the smallest possible polygons according to major tectonic zones as defined by previous researchers (Le Pichon and Angelier, 1979; Le Pichon et al., 1995; Kahle et al., 1998; Papazachos et al., 1999). Following this, neighboring polygons with similar strain rates are merged. We tried to ensure that each final polygon bounds the whole of either a main fault zone or a trough zone. This was not always possible, because the faults can be quite small or concentrated in a narrow area (e.g. Corinth Gulf, Evia Gulf). In the final polygons, the uniform strain is a good fit (in terms of the root mean square weighted residual) to all the stations that pertain to it. In total, 22 polygons were formed. The principal horizontal

277 strain rates and their formal errors, for each of the chosen polygons, are computed using
278 the program *polystr2* (Clarke, 1996).

279 Table 4 and Figure 7 summarize the results for each polygon, and Figure 8
280 presents the geodetic rigid body rotation for each of the 22 polygons. In some cases there
281 is a large uncertainty in the azimuth of the principal strain rates, although their
282 magnitudes are relatively certain. This occurs if strains are small compared with their
283 formal errors, or if the principal strain rate components are roughly equal (in the limit of
284 exact equality the azimuth is undefined). However, if the two principal strain rate
285 components differ considerably, with one being much larger than the other, then the
286 azimuth will be well determined. Clockwise rotation is observed around the North
287 Eastern Aegean, Gulf of Corinth, and Gulf of Evia, with the rates decreasing around the
288 Grevena and Chalkidiki areas. The sense of rotation changes in the South Aegean and
289 Cyclades area where anti-clockwise rotation is present.

290 In the North Eastern Aegean region the results show a dominant extensional
291 deformation in the ENE-WSW direction of around 0.2±0.06 ppm/yr (polygon 22). This
292 extensional deformation turns to a NNW-SSE direction further to the west and the
293 Chalkidiki area (polygon 21). This extension is suggested by Kahle et al. (1998; 1999;
294 2000), but for their case the deformation is even stronger, reaching 0.205 ppm/yr at the
295 western end of the North Anatolian Fault (NAF) and 0.15 ppm/yr at the North Aegean
296 Trough. Straub et al. (1997) use GPS data to determine the strain rate pattern at the
297 western end of the NAF, and conclude on an average value of 0.11 ppm/yr for the whole
298 Marmara region with a maximum value of 0.31 ppm/yr.

The Grevena area (polygon 20) is previously thought as aseismic region but here it appears to extend in a NNW-SSE direction (~0.07 ± 0.02 ppm/yr) with a small degree of shortening. Theodulidis (1998) suggests after observing macroseismic intensities and strong motion data following the 1995 Kozani-Grevena earthquake that in this area there are seismic faults that may be unknown or considered as non-active but still capable of generating destructive earthquakes. This is an area where the lack of contemporary or historical seismic activity can indicate 'hazard' rather than safety (Pavlides et al., 1995; Meyer et al., 1996; Pantosti et al., 1996; Chatzipetros et al., 1998; Pavlides and King, 1998; Pavlides and Caputo, 2004). Polygon 7 is centered on the Gulf of Patras and western Corinth Gulf, east-west compressional deformation combines with north-south extension to give right lateral transpression. The east-west compression increases towards the entrance of the Gulf of Patras from 0.13±0.08 ppm/yr (polygon 6) to 0.24±0.11 ppm/yr (polygon 7). Shortening has been pointed out by Kahle et al. (1995) who suggest a pure compressional tectonic stress dominant in the Gulf of Patras in E-W direction. Davies et al. (1997) suggest a predominant contraction in the Pindos mountains and Epirus region to the west.

The Gulf of Corinth and the Gulf of Evia are major grabens bounded by faults that are segmented and not continuous for more than 15-20 km. Both gulfs have been tectonically active since the Quaternary and have experienced intense earthquake activity in the last century (Ambraseys and Jackson, 1990), although earthquake activity in the Gulf of Evia has been lower in the last 30 years. In the Corinth Gulf, most historical activity has occurred within a seismogenic belt that is 30 km wide by 130 km long between Corinth and the Patras area (Roberts and Koukouvelas, 1996). Here, WSW-

trending normal faults are accommodating most of the N-S extension (Doutsos and Piper, 1990; Jackson, 1994). Studies in the area of the Gulf of Corinth, have been investigating the tectonic evolution as well as the mechanism related to the seismicity resulted by these onshore and offshore faults. Two different tectonic phases seem to be responsible for extreme complexity of the structure of the region. The first one is represented by the Cenozoic E-W compressional phase, which gave rise to the Hellenic orogenic belt. The second tectonic phase is represented by the extension of the Aegean region, which started in Miocene time. This phase was initially characterized by a predominant NE-SW direction in the Corinth region. During the Quaternary, The Aegean extension was accelerated by the southwestward propagation of the NAF, which has reactivated features from the first tectonic period approximately 1Ma. (e.g Armijo et al., 1996; Rigo et al., 1996; Bernard et al., 1997; Clarke et al ., 1997; Briole et al., 2000; Moretti et al., 2003; Latorre et al., 2004; Lyon-Caen et al., 2004). The results here show a dominant extension rate present around the Corinth Gulf (polygon 8) 0.24±0.22 ppm/yr in an almost N-S direction also pointed out by Hollenstein et al. (2008). The extension rates are lower around the Gulf of Evia, 0.11±0.4 ppm/yr in an E-W direction. Around the Saronic Gulf (polygon 11) the extension rates turn in an NE-SW direction at 0.1±0.1 ppm/yr. In Attiki (polygon 12) extension and compression are both present giving shear, while in the Saronic islands (polygon 1) we have pure extension of 0.28±0.16 ppm/yr in a NNE-SSW direction. The fact that the maximum extensional strain is perpendicular to the strike of the Corinth Gulf is in agreement with the strain shown in the focal mechanisms of earthquakes (Ambraseys and Jackson, 1990). According to Clarke et al. (1998) there may be fewer active fault segments taking up the strain across the gulf of Evia and it is

345 possible that earthquake recurrence times on individual fault segments in the Gulf of
346 Corinth are shorter to accommodate higher strain rates in the underlying lithosphere.
347 According to Kahle et al. (1998; 1999; 2000), in central Greece the maximum extensional
348 components of the strain rate tensor are centered around the Gulf of Corinth in an almost
349 N-S direction.

350 The central Aegean undergoes a NE-SW extensional deformation of
351 0.08±0.05ppm/yr. The Cyclades area is almost strain free. The strain free Cyclades area
352 has been suggested by other researchers in the past again based on GPS measurements.
353 Kahle at al., 1998 while estimating the strain rate field in the eastern Mediterranean
354 region with repeated GPS measurements, conclude that there is a relative strain free
355 region in the south-central Aegean, between the volcanic and non-volcanic Greek-
356 Hellenic arc. Kahle et al., 1999 return to the subject and suggest that the SW Aegean Sea
357 and central Anatolia are almost strain-free adding that these strain free regions are nearly
358 aseismic. They conclude by saying that the Cyclades islands are almost strain-free and
359 show low seismicity. Jenny et al., 2004 refer to the southern Aegean region as a low
360 straining region where deformation occurs mostly aseismically. Very thin lithosphere due
361 to extension and hydration by the subduction slab probably limits the seismogenic
362 thickness. The Sea of Crete in its eastern part (polygon 18) extends in a NNE-SSW
363 direction while its western part (polygon 17) extends NE-SW. These two polygons rotate
364 differently. This agrees with what has been suggested by Kahle et al. (1998; 1999; 2000),
365 that the area of the South Aegean Sea (around the Dodecanese islands with principal
366 extension value of around 0.09 ppm/yr) is probably related to tectonic processes in the
367 SW Anatolia graben system accompanied by recent volcanic activity. Recently Kokkalas

and Doutsos (2001) suggest that the area from eastern Crete to the Dodecanese islands (an area further south than our grid cover) display an arc-parallel extension combined with sinistral shear due to oblique convergence in the area.

The deformation seems to ease out in Peloponnisos (polygons 2, 3, 4). In polygon 3 low levels of extension and compression are present while in polygon 2 there is only pure NNE-SSW extension of around 0.04±0.1 ppm/yr. In the Messinia Gulf (south Peloponnisos, polygon 4) low levels of extension are present, while strong compression is shown (0.3±0.27 ppm/yr) between the Laconia Gulf and the island of Kythira (polygon 19). Both of these gulfs are bounded by active faults.

4.2 Minimum curvature strain analysis

This second method of deriving horizontal geodetic strain rates is independent of geological preferences, depending only on the velocity field data. We fitted a continuous minimum-curvature surface to the east and north site velocity datasets in turn, allowing interpolation between points. The method has been analyzed in detail by Smith and Wessel (1990) and has been applied in different parts of the world to describe deformation patterns (e.g., Chang et al., 2003). This interpolation process puts strong emphasis on the nearby measurement point as compared with distant ones, which allows better characterization of local variations in the rate of deformation field. Three different grid spacing values were tested (20, 30, 40 minutes). To optimize grid spacing without over-fitting the data, we computed a chi-square statistic for each fit (mean square weighted residual). The 20 minute grid gave a result of 0.23, the 30 minute grid gave a result of 0.50, and the 40 minute grid gave a result of 0.54. Despite its lower statistic, the

20 minute grid did not show any regions of visibly different strain patterns when compared with the 30 minute grid, whereas the 40 minute grid masked detail that was observed with the 30 minute grid. Therefore the 30 minute grid spacing was chosen. The continuous east and north velocity fields were then differentiated to give the velocity gradient tensor, from which principal strain and rotation rates were computed (Figure 9). The comparison between the two strain determination methods showed very good agreement. In Figure 10 the average strain rate for each polygon as determined from the polygon method is compared with the point values taken at the centroid of each polygon as derived by the minimum curvature method.

Grevena, northern Greece, central Aegean, and Sea of Crete areas show agreement in both the direction and magnitude of deformation. The same applies for western Greece, the Patras area and western Corinth Gulf, the central Corinth Gulf and SW Peloponnisos (polygons 3, 4). Cyclades (polygon 16) appear strain free in both methods. Polygon 19 (the Gulf of Laconia) deforms differently for both methods. An obvious difference in the direction of deformation is observed around the northern Gulf of Evia where the type of deformation is extension ~ 0.11ppm/yr. In the polygon method (see polygon 10) the direction of deformation appears as E-W while in the gridding method the direction of deformation appears as NNW-SSE. A difference in direction also exists for polygon 11 (Saronic Gulf). Compression is observed for polygon 12 (Attiki) in both methods but for the gridding method there is no extension for this area. These differences can be explained because in the polygon method the azimuth often appears with large uncertainty, particularly if the polygon has a large aspect ratio. In the gridding method data from the wider region will have an influence, and so small differences in

414 velocity between closely-spaced sites are less likely to cause large errors. The geodetic
415 rigid-body rotation rates show a similar pattern for both the methods applied. Strong
416 clockwise rotation is observed in the Peloponnisos area, central Greece and the northern
417 Aegean Sea, while strong counter-clockwise rotation is observed in the central Aegean,
418 Cyclades, and Sea of Crete.

419 These results agree well with previous studies that took place in the eastern
420 Mediterranean region. Taymaz et al. (1991) noted the predominance of strike-slip
421 faulting in the northern Aegean and extension in central Greece and proposed a broken-
422 slat model where central Greece rotates clockwise and the southern Marmara slats rotate
423 counter-clockwise. This admittedly simplistic configuration of nine broken-slat
424 microplates model is now recognized not to be quantitatively comparable with the full
425 velocity field. Le Pichon et al. (1979; 1995) proposed a two block model where central
426 Greece (north of the Gulf of Corinth) rotates clockwise and the south Aegean and
427 Anatolia rotate counter-clockwise. Extension is observed across the Gulf of Corinth and a
428 wide zone of distributed strike-slip deformation is present in the northern Aegean.
429 McClusky et al. (2000) define rigid blocks in central Anatolia and the southern Aegean.
430 The SE Aegean region rotates counterclockwise and moves towards the Greek-Hellenic
431 trench (i.e., toward the SE). They suggest that much of the Aegean is deforming by
432 distributed extension that is widespread in Greece and in the northern Aegean Sea. For
433 the Greek area they included data from observations in the Aegean region (1988-south,
434 1989-north, 1992-all, and 1996-all) and also data from the Western Greek Arc as these
435 are described in Kahle et al. (1996). Coverage in Central Greece and other sensitive areas
436 such as gulf of Argos, Grevena, Evia that need special attention was poor. Armijo et al.

(1996) propose that lower rates of extension occur across a small number of discrete zones in the central Aegean and SW Anatolia. Most of the Aegean, Greek Arc and Peloponnisos are extruded in SW direction. Propagation of the southern branch of the NAF across the Aegean may have progressively reactivated the Skyros island, the northern Evia basin, the Evia graben, and finally the Corinth rift. Accelerated clockwise rotation may occur within Peloponnisos and central Greece. The kinematic model that they proposed emphasized the extensional end effects of the right-lateral termination of the NAF in the NW Aegean and central Greece.

5. Seismic hazard estimation

5.1 Methodology

The next step of our analysis is to compare the strain rate values obtained through geodetic measurements with those derived from recorded seismic events that took place in the Greek area. Various studies have been conducted in different parts of the world performing this comparison between seismicity and geodesy (Ward, 1998a, 1998b; Shen Tu et al., 1998; Kreemer et al., 2000; Masson et al., 2005; Pancha et al., 2006). The dense geodetic data distribution, relatively long historical catalogues and high activity rates make this region ideal for constructing independent measurements of seismic and geodetic strain rates. We map seismic strain rates in the same grid as used for the geodetic field. A key question is what duration of earthquake catalogue is most suitable for relating seismic to geodetic strain, at the spatial scales that we have observed the latter and if the bulk of the tectonic strain in this region is released by seismic slip on faults. Seismic moment rates that are low compared with tectonic strain rates may indicate that

460 deformation occurs in part aseismically, which has been suggested previously (Jackson
461 and McKenzie, 1988; Briole et al., 2000; Jenny et al., 2004).

462 To derive the seismic strain rate we used three earthquake catalogues (Figure 11).
463 In general, the smaller the area under investigation the longer the sample time must be for
464 a representative seismic moment rate to be derived (Ambraseys and Jackson, 1997). We
465 used the Global Centroid Moment Tensor (GCMT) catalogue (http://www.globalcmt.org,
466 former Harvard CMT) that covers the whole of the Greek area for magnitudes greater
467 than ~4.5 and goes back to 1976; the Ambraseys and Jackson 100-year catalogue (1890-
468 1988) complete for M_S>5.8 for central Greece (Ambraseys and Jackson, 1990); and
469 finally the Ambraseys and Jackson 300-year catalogue (1694-1995) that covers the
470 Corinth area for M_S>6.0 (Ambraseys and Jackson, 1997). The Ambraseys and Jackson
471 (1997; 1990) studies even though they extensively covered the seismicity surrounding
472 prominent, active geological structures, have not been (as far as we know) compared to
473 geodetic results.

474 In order to determine if there is any imbalance between geodetic and seismic
475 strain rates we assign the seismic events from each of the three catalogues to the
476 polygons as defined in Figure 7. All three catalogues refer to crustal earthquakes (depth ≤
477 40 km). For our area of research the GCMT catalogue includes events with surface wave
478 magnitude M_S≥4. The 100-year catalogue includes events with M_S ≥5.8 and the 300-year
479 catalogue includes events M_S≥6.0. Events with large M_S are the ones which are actually
480 of interest here, because these release the majority of the strain and consequently are
481 responsible for much of the deformation. To estimate seismic strain reliably, accurate
482 knowledge about the rates of recurrence of moderate size events (Mw= 4.5-6.5) is

needed. For b ≥ 1, these events can accommodate 60 per cent of the strain (Jenny et al., 2004). In order to estimate the strain accounted as seismicity during the three different periods covered by the catalogues we used the technique of Kostrov (1974). The seismic moment tensors are constructed from the fault plane solution (strike, dip, and rake) and scalar seismic moment $M_{0,}$ for each of the events. We used a seismogenic layer thickness of 10-15 km as is commonly assumed as a reasonable estimate of the depth range over which the bulk of the seismic strain is accommodated in continental areas (Taymaz et al., 1991; Rigo et al., 1996; Jenny et al., 2004). The Cartesian components of $\boldsymbol{M}$ (moment tensor) for a double-couple event described by the strike ϕ_s, the rake λ, dip δ and moment M_0 are obtained as described in Aki and Richards (Page 112, Box 4.4) (2002). For the GCMT catalogue the moment magnitude Mw has already been computed (using the formula of Kanamori (1977)). For the other two catalogues the seismic moment M_0 values were calculated from the M_S values using the most recent formulas given for the eastern Mediterranean by Ambraseys (2001). Table 5 presents the seismic strain rates results for the three catalogues, using seismogenic layer thicknesses of 15 km (for the 10 km thickness these values need to be multiplied by 1.5; Rontogianni, 2007).

5.2 Application and results

For the 30-year catalogue (Figure 12 a) the seismic strain rate in polygons 20 (Grevena) and 9 (western central Greece) is large, and especially for polygon 9 exceeds that of the geodetic strain. This is not observed in the two longer catalogues (Figure 12 b, and Figure 12 c). When seismic strain is larger than the geodetic strain it implies that the observed earthquakes release strain accumulated over longer periods than the seismic

strain rates are calculated (i.e. the period covered by each catalogue). Another explanation may be that the area covered by a polygon may be small but has a large seismic moment rate caused by a single very strong earthquake. That is exactly what happens for polygon 9, which is quite small but includes the July 1980 earthquake with M_S=6.4. Polygon 20 surrounds the area most influenced by the May 1995 Kozani-Grevena earthquake with M_S=6.6, this area was previously considered to be of low seismic risk (Papazachos, 1990). This is strongly suggested by the surrounding polygons where there is negligible amount of recent seismic strain release (e.g. polygon 6). Polygon 11 also has a large amount of seismic strain caused by the 24 February (M_S=6.7) and 25 February (M_S=6.4) 1981 Alkyonides earthquakes (Leeder et al., 2005). Polygon 11, which surrounds the Saronic Gulf and east Corinth area, appears to have a significant rate of seismic strain release for all of the 3 catalogues. Polygon 8 (central Gulf of Corinth) has a high level of seismic strain which is not surprising since it includes the 18 November 1992 earthquake with M_S=5.9 and the 15 June 1995 Egion earthquake with M_S=6.2. Both these events are, unfortunately, not included in any of the other two, older, catalogues. From this we can infer that a 30 years period is not capable to describe fully the seismic strain rate at the scale of chosen polygons and it is highly affected by the magnitude of the events that struck the area during the 30-year interval.

The 100-year catalogue reaches 1988 which means that it does not include all of the above-mentioned earthquakes. In this catalogue the seismic deformation is distributed amongst the majority of the polygons with only the Saronic – east Corinth area (polygon 11) having a considerably higher amount of seismic strain release. Polygon 12 appears to have released a great amount of seismic strain. In this polygon we have placed

the 1955, M_S=5.9 earthquake. Unfortunately this is an event that is placed directly on the margins between polygon 11 and polygon 12 which means that it could equally well be included in polygon 11. It is not an event that exists in any of the other catalogues since the 300-year catalogue includes $M_S \geq 6$ and the 30-year catalogue goes back only to 1977. Even the 100-year catalogue is insufficient to reveal all the major active tectonic structures, and any assessment of seismic risk should take a longer perspective. This suggestion is also supported by Ambraseys (1990). For the same catalogue, Davies et al. (1997) suggested that whereas seismic strain in the eastern Gulf of Corinth is commensurate with the geodetic strain, there is a rapid extension across the western Gulf of Corinth with negligible seismic strain. They concluded that this is consistent with the deformation that would be expected of a sheet of fluid moving towards a low-pressure boundary at the Greek-Hellenic Trench.

For the 300-year catalogue it can be suggested that there is an amount of seismic activity present in polygons 7, 8, and 11, but nonetheless lower than the geodetic strain. Polygon 7 appears free of seismic strain in both the 100 and 30-year catalogues but appears with a considerable amount in the 300-year catalogue. Polygon 8 (central Gulf of Corinth) has increased its seismic strain release rate from the 100-year catalogue but has decreased with respect to the 30-year catalogue. Finally, the relatively large polygon 11, which lies in a highly active region, has similar seismic strain release rates for all three catalogues. However, for the other, generally smaller or less straining polygons, it can be suggested that the 300-year catalogue best describes the area at the scale of these polygons and is less influenced by individual events or polygon sizes. Ward (1998 a, b)

551 while working in data sets from Europe and the United states suggested that short
552 catalogues are more likely to underestimate than overestimate long-term moment rates.

553 The above observations indicate where unreleased strain is accumulating in an
554 area, but cannot predict when or how this strain will be released. It is fortunate that for
555 the Corinth area, macroseismic evidence exists for events of the pre-instrumental period
556 to assess seismicity and compare with more recent catalogues of events (100 years and 30
557 years). It is difficult to assign a given earthquake to a fault even with modern data.
558 According to Pavlides and Caputo (2004) it is possible due to large recurrence intervals
559 the fault or the fault system responsible for earthquakes to be unidentified and the
560 potential danger underestimated. Ambraseys and Jackson (1990) suggest that the typical
561 time interval between occurrences of major earthquakes on a fault in this region certainly
562 exceeds 100 years and possibly even 1000 years in some of the more slowly straining
563 parts of the region. That is supported by palaeoseismological studies in Greece that have
564 shown the average recurrence interval of specific active faults to be commonly longer
565 than 500 years and usually some thousands years (Pantosti et al., 1996; Chatzipetros et
566 al., 1998). For the Kaparelli, Eliki and Egion faults, all located with the Gulf of Corinth,
567 the mean recurrence intervals that have been suggested are 2520 years, 900-400 years (or
568 270-1200 years according to Koukouvelas et al. (2001)) and 360 years respectively, for
569 the Paleohori-Sarakina fault (near Kozani area) this interval is 30.000 years (Pantosti et
570 al., 2004; Chatzipetros et al., 2005; Kokkalas et al., 2007).

571 There are several parameter values that have to be assumed in order to derive the
572 seismic strain, which contributes to the uncertainty in the above results. For the seismic
573 rates estimated from the historical earthquake catalogues to be valid, the average

recurrence interval is required to be shorter than the historical record. For an individual fault a complete earthquake cycle is required. Alternatively, for a region containing multiple faults, the historical seismicity record is required to be long enough to capture a statistical sample of all phases of the seismic cycle, including of course earthquakes, but different parts of the cycle can be represented by different faults. With this constraint, the catalogue duration is almost always too short to give a reliable occurrence rate estimate for regions the size of an urban area, as desired for detailed seismic-hazard analysis. Pancha et al. (2006) support the hypothesis that even a few years of detailed geodetic monitoring can provide a good constrain on earthquake occurrence rate estimates for large enough regions. Ward (1998 a) suggests that median catalogues of 200–300 years duration are adequate for regions straining at 10^{-7} yr^{-1}, for regions straining at 10^{-9} yr^{-1} more than 20.000 years of earthquake data are needed. For geodesy to give reliable estimates two conditions are necessary. First, the geodetic measurements should sample a large enough spatial scale so that they are not affected by non-linear strain accumulation during the earthquake cycle on individual faults. Second, they should sample a long enough time interval that measurement uncertainties have a minimum effect on the estimated velocities. Our analysis takes the two steps under consideration. Pancha et al. (2006) propose that if the deformation rate is fast enough then there can be a meaningful comparison of average strain rates. The distributed seismicity of the region is assumed to be caused by a sufficient number of faults at different stages of the earthquake cycle to compensate for the long recurrence interval of individual faults. According to these suggestions the comparison between the two strain rates can be applied with meaningful results for Greece. Geodetic and seismic measurements sample different aspects of the

deformation field. Seismic and geological estimates serve only as a record of brittle deformation, whereas geodesy encompasses both seismic and aseismic strain accumulation. Geodetic rates cannot uniquely determine slip at depth and may only give a measure of the instantaneous strain transients, which may not be preserved throughout the earthquake cycle (Savage and Lisowski, 1998; Shen-Tu et al., 1999). The final uncertainty arises in converting strain rates in seismic moment rates. Field et al. (1999) also analyze in detail factors that contribute to uncertainties in estimates of long term seismic moment rate from historical catalogues. The greatest uncertainty comes from: a) the M_0 – M_S relation used to obtain the seismic moment, b) the assumption of the effective seismogenic layer thickness; 10 km and 15 km represent reasonable lower and upper bounds on this, c) in the 100-year and 300-year catalogues, only the larger events that took place in the Greek area are included; it has been suggested (Ambraseys and Jackson, 1990) that the smaller events (with $M_S \leq 5.8$) may contribute to and increase the displacement in the central Greece area by up to 50 per cent.

For the majority of the polygons in this study the geodetic strain is larger than the seismic strain, which implies that a strain deficit may be released by earthquake activity at some point. That difference between geodetic and seismic strain rates has been suggested also by Ward (1998b) when working with data from Europe. According to the geodetic measurements there is a high rate of deformation in the Gulf of Patras-western Corinth Gulf (polygon 7) and central Gulf of Corinth (polygon 8), of which less than half has been released by seismic strain. However, this strain need not necessarily be released by very large earthquakes, even though the Corinth area has given M_S= 6.7 (24 February 1981) earthquake in the past, but could be released by many small earthquakes (Clarke et

al., 1997). Equally, we cannot be certain that aseismic deformation does not happen, since aseismic creep has been observed in other parts of the Mediterranean region and the Greek-Hellenic Trench (Jackson and McKenzie, 1988, 1988a). A continuous aseismic deformation in the uppermost crust of the Corinth rift has been suggested by Briole et al. (2000). Jenny et al. (2004) suggested that the major strike-slip zones in the region, the Northern Anatolian Fault and the Kephalonia Fault, experience little to negligible aseismic deformation. In the remaining eastern Mediterranean up to 10–30 per cent of the total deformation is aseismic. The Hellenic Trench is largely uncoupled, with at least 50 per cent and up to 90 per cent of the compressive strain released aseismically.

5.3 Consistency of velocity field with orientation of faulting

Faults in the upper crust are shear fractures and represent therefore, lines parallel to which there is no local change of length. We examine the orientation of faulting which is capable of accommodating the observed distribution of geodetic strain rates and whether the calculated orientation of faulting is consistent with the input fault orientation as given in seismic catalogues. Holt and Haines (1993) suggested that, if there are no variations in the magnitude of fault slip along the direction parallel to strike, then the only orientations of faulting that can reproduce the horizontal components of the strain tensor correspond to the directions of no length change in the velocity field. These directions are equivalent to the strikes of the nodal planes from any fault plane solution compatible with the local horizontal strain tensor (Bourne, 1996). Figure 13 presents the predicted strikes of faulting calculated from the continuous-curvature velocity field (black symbols) together with the fault plane solutions (red symbols) from the combination of the three

643 seismic catalogues. Where the events overlap we kept the ones from the more recent
644 catalogue. For the GCMT catalogue we used only the events with $M_S \geq 5.5$. We see close
645 agreement between the orientations of the larger faults as calculated from the strain rate
646 field and lines of no length change (Figure 13). These areas are the North Aegean
647 (extension of North Anatolia Fault Zone), Skyros island, Gulf of Evia, Epirus area,
648 Saronic Gulf and Gulf of Argos. We observe problems in matching orientations in the
649 area surrounding the Gulf of Corinth. The main reasons of misalignment have been
650 analyzed by England and Molnar (1997) and Holt and Haines (1993) while applying the
651 technique in Asian data. According to these authors the misalignment can result either
652 from the local orientations of faults being controlled by pre-existing weaknesses of the
653 crust or because in these areas the strain field changes rapidly over short distances. Both
654 of these explanations can relate to the Gulf of Corinth, Armijo et al. (1996) suggested two
655 different phases of deformation with the later (1 Myr) reactivating a pre-existing earlier
656 phase (15 Myr ago or earlier) his suggestion is supported by more recent
657 geomorphologic, stratigraphic and microseismicity studies (Goldsworthy and Jackson,
658 2001; Lyon-Caen et al., 2004). From our analysis we also showed that the strain pattern
659 does actually change rapidly as we move from the east to the west of the Corinth Gulf in
660 a 120 km long and up to 30 km wide area. We can also add that the catalogues include
661 only relatively few earthquakes, which may not be entirely representative of the longer-
662 term seismic character (indeed, the discrepancy between geodetic and seismic strain also
663 suggests this).

In order to investigate the level of agreement, we derived a quantitative estimate of the difference between the geodetic directions of no length change and the fault plane azimuths ϕ ($0^\circ \le \phi \le 90^\circ$) using:

$$\phi = \cos^{-1}\left|\sin\theta_s \sin\theta_g + \cos\theta_s \cos\theta_g\right| \qquad (2)$$

where θ_s is the strike as given in our combined seismic catalogue and θ_g is the strike calculated from the continuous velocity field.

For the older catalogues only one of these fault planes is given and must be matched with the appropriate no-length-change direction; for the GCMT catalogue, where both conjugate fault planes are given, we use the better-fitting of the two directions. For the combined 300 and 100 year catalogues, the mean absolute difference in orientation is 32°, and for the GCMT catalogue it is 35°.

In view of the close agreement between the orientations of the larger faults and of lines of no length change we conclude that the comparison is possible and the orientation of active faulting compares well with the configuration required to accommodate the present-day distribution of strain rates. The fact that the active faults accommodate the present-day regional strain rates increases the likelihood that the geodetic-seismic strain deficit will be released by future earthquake activity in this area.

5.4 Correlation of results with seismicity from 2000-2008

Our conclusions derived from the reprocessing and analysis of the old campaign GPS data, can be justified by the seismicity as this developed from 2000 till 2008 (Figure 14). The events plotted are from the GCMT and have Mw≥5.0. From Figure 14 is shown that in the polygon 7 we have 4 events during this 8 year period. Three events occurred in

April 2007 with Mw 5.0, Mw 5.1 and Mw 5.2 at 15 km depth (Evangelidis et al., 2008). The forth event occurred in June 2008 with Mw 6.4 located at 22 km depth (Konstantinou et al., 2009). Konstantinou et al. mention a possibility of reactivation of a fault structure inherited by previous tectonic phases based on the fault depth and strike. This earthquake activity justifies our conclusion according to which there is a high rate of deformation in the Gulf of Patras (polygon 7) and central Gulf of Corinth (polygon 8), of which less than half has been released by seismic strain. For polygon 7 seismic strain rates are observed in the 300-year catalogue that are not observed in the 100 and 30-year catalogues. Large events are also located in central Aegean (polygon 14). In July 2001 an event with Mw 6.4 occurred in the North Aegean Sea, this event mainly affected the area around the Skyros island. This area is only covered by the 30 and 100 year catalogues, nevertheless polygon 14 is characterized by strong extension and in both catalogues the geodetic strain rates are larger than seismic strain rates. We also show that the North Aegean (extension of North Anatolia Fault Zone) and Skyros island are areas where there is a close agreement between the orientations of the larger faults as calculated from the strain rate field and lines of no length change so that deficit can be expressed by seismicity. Papadimitriou and Sykes (2001) while evaluating the evolution of the stress field in the northern Aegean Sea, extrapolate their results to the year 2020 suggesting that the region north to Skyros island as one of the three possible candidate areas where large events are more likely to occur.

6. Conclusion

709 In this work a complete processing of 6 years of campaign-type GPS data was
710 performed.

711 • 18 GPS campaigns were successfully combined including areas not fully covered
712 previously. Through the whole study a consistent processing approach was
713 followed and for better reference frame definition the local sites were combined
714 with IGS and EUREF sites.

715 • In a Eurasian reference frame sites around the Chalkidiki and Grevena areas show
716 a small residual motion of around 10 mm/yr. Sites around Attica, Evia, and the
717 eastern and southern Peloponnisos, as well as the Aegean islands, have a SW
718 motion which increases from ~25 mm/yr for the Aegean islands to around 30
719 mm/yr around Attica, Evia and the eastern Peloponnisos coast and ~40 mm/yr for
720 sites in the southern Peloponnisos. The Patras area shows a residual motion of
721 around 30-35mm/yr.

722 • The central and south Aegean are extending but the Cyclades area is almost strain
723 free. The Grevena area previously thought as aseismic appears to extend in a
724 NNW-SSE direction. The Gulf of Patras and western Corinth Gulf have east-west
725 compressional deformation combined with north-south extension. The
726 compression increases towards the entrance to the Patras Gulf and western
727 Greece. North-south extension is dominant in the Corinth Gulf area. The Evia
728 Gulf appears with a lower degree of extension when compared with the Corinth
729 Gulf. For the Saronic gulf there is pure extension in a NNE-SSW direction.
730 Clockwise rotation is observed in central Greece around the Gulfs of Corinth and

731 Evia, turning to anticlockwise rotation in the south Aegean and southern
732 Peloponnisos.

733 • For the seismic hazard determination the geodetic and seismic strain rates were
734 compared. From the three earthquake catalogues used, the 300-year catalogue is
735 less influenced by individual events or polygon sizes. The Saronic Gulf-eastern
736 Corinth area has a consistent, low degree of seismic strain release in all three
737 catalogues. The Gulf of Patras and western Gulf of Corinth (polygon 7) appear to
738 be undergoing seismic deformation for the 300-year catalogue at a higher rate
739 than observed in the 100-year catalogue. For the majority of Greek region the
740 geodetic strain rates are larger than the seismic strain rates. This suggests that
741 accumulated strain has not been released yet by earthquake activity.

742 • Close agreement is observed between the orientations of the larger faults as
743 calculated from the strain rate field and lines of no length change. These areas are
744 the North Aegean (extension of North Anatolia Fault Zone), Skyros island, Gulf
745 of Evia, Epirus area, Saronic Gulf and Gulf of Argos. Orientation mismatching
746 around the Gulf of Corinth is explained by pre-existing weaknesses of the crust
747 and the rapid change of the strain field over short distances. The fact that the
748 active faults accommodate the present-day regional strain rates enhances the
749 likelihood that the geodetic-seismic strain deficit will be released by future
750 earthquake activity in this area.

751 • Our analysis conclusions were verified by the earthquake activity that followed
752 the study from 2000-2008 where in polygon 7 four events occurred with Mw 5.0,
753 Mw 5.1, Mw 5.2 and Mw 6.4.

Acknowledgements

We thank staff and students of numerous institutions who have taken part in the field GPS campaigns on which this analysis is based. Michael Floyd (Oxford University) is thanked for his contribution in processing the Egion campaigns using GAMIT. P.J. Clarke and M.A. King from School of Civil Engineering and Geosciences, Newcastle University, UK, are thanked for their suggestions made during preparation of the manuscript. D.A. Lavallée, Faculty of Aerospace Engineering, Delft University of Technology, for his assistance in using TANYA and commenting on earlier drafts. We acknowledge the very useful comments and suggestions from K.I. Konstantinou, Institute of Geophysics, National Central University, Taiwan, S. Kokkalas and an anonymous reviewer. Support of the author by the Taiwanese National Science Council is greatly appreciated.

766
767
768 **References List**

769 Aki, K., Richards P. G., 2002. Quantitative seismology, University Science books, Sausalito,
770 California.

771

772 Altamimi, Z., Sillard, P., Boucher, C., 2002. ITRF2000: A new release of the International
773 Terrestrial Reference Frame for earth science applications. J. Geophys. Res. 107(B10), 2214.
774 doi:2210.1029/2001JB000561.

775

776 Ambraseys, N., 2001. Reassessment of earthquakes,1900-1999, in the Eastern Mediterranean and
777 the Middle East. Geophys. J. Int. 145, 471-485.

778

779 Ambraseys, N., Jackson, J., 1997. Seismicity and strain in the Gulf of Corinth (Greece) since
780 1694. J. Earthq. Eng. 1(3), 433-474.

781

782 Ambraseys, N., Jackson, J., 1990. Seismicity and associated strain of central Greece between
783 1890 and 1988. Geophys. J. Int. 101, 663-708.

784

785 Angelier, J., Lyberis, N., Le Pichon, X., Barrier, E., Huchon, P., 1982. The tectonic development
786 of the Hellenic arc and the Sea of Crete: a synthesis. Tectonophysics. 86, 159-196.

787

788 Armijo, R., Meyer, B., King, G.C.P., Rigo, A., Papanastasiou, D., 1996. Quaternary evolution of
789 the Corinth Rift and its implications for the Late Cenozoic evolution of the Aegean.
790 Geophys. J. Int. 126, 11-53.
791
792 Ayhan, M. E., Demir, C., Lenk, O., Kilicoglu, A., Altiner, Y., Barka, A., Ergintav, S., Ozener,
793 H., 2002. Interseismic strain accumulation in the Marmara Sea region. Bull. Seismol. Soc.
794 Am. 92 (1), 216-229.
795
796 Bernard, P., Briole, P., Meyer, B., Lyon-Caen, H., Gomez, J-M., Tiberi, C., Berge, C., Cattin, R.,
797 Hatzfeld, D., Lachet, C., Lebrun, B., Deschamps, A., Courboulex, F.,, Larroque, C., Rigo, A.,
798 Massonnet, D., Papadimitriou, P., Kassaras, J., Diagourtas, D., Makropoulos, K., Veis, G.,
799 Papazisi, E., Mitsakaki, C., Karakostas, V., Papadimitriou, E., Papanastassiou, D.,
800 Chouliaras, M., Stavrakakis, G., 1997. The M_s=6.2, June 15, 1995 Aigion earthquake
801 (Greece): evidence for low angle normal faulting in the Corinth rift. J. Seismol. 1, 131-150.
802
803 Beutler, G., Bock, H., Brockmann, E., Dach, R., Fridez, P., Gurtner, W., Hugentobler, U.,
804 Ineichen, D., Johnson, J., Meindl, M., Mervart, L., Rothacher, M., Schaer, S., Springer, T.,
805 Weber, R., 2001. Bernese GPS software Version 4.2, Astronomical Institute, University of
806 Berne 2001.
807
808 Billiris, H., Paradissis, D., Veis, G., England, P., Parsons, B., Cross, P., 1991. Geodetic
809 determination of the tectonic deformation in central Greece from 1900-1988. Nature 350
810 (6314), 124-129.

Blewitt, G., Lavallée, D.A., 2002. Effect of annual signals on geodetic velocities. J. Geophys. Res. 107(B7), 2145. doi:10.1029/2001JB000570.

Bohnhoff, M., Rische, M., Meier, T., Becker, D., Stavrakakis, G., Harjes, H-K., 2006. Microseismic activity in the Hellenic Volcanic Arc, Greece, with emphasis on the seismotectonic setting of the Santorini-Amorgos zone. Tectonophysics 423, 17-33. doi:10.1016/j.tecto.2006.03.024.

Bourne, S. J., 1996. Distributed deformation of the South island of New Zealand, Faculty of Physical Sciences. PhD Thesis, University of Oxford, Oxford.

Briole, P., Rigo, A., Lyon-Caen, H., Ruegg, J.C., Papazissi, K., Mitsakaki, C., Balodimou, A., Veis, G., Hatzfeld, D., Deschamps, A., 2000. Active deformation of the Corinth rift, Greece: Results from repeated Global Positioning System surveys between 1990 and 1995. J. Geophys. Res. 105 (B11), 25,605-25,625.

Bruyninx, C.,Becker, M.,Stangl, G., 2001. Regional Densification of the IGS in Europe Using the EUREF Permanent GPS Network (EPN). Phys. Chem. Earth Pt. C. 26, 531-538.

Chang, C. P., Chang, T.Y., Angelier, J., Kao, H., Lee, J.C., Yu, S.B., 2003. Strain and stress field in Taiwan oblique convergence system: constraints from GPS observations and tectonic data. Earth Planet. Sci. Lett. 214, 115-127. doi:10.1016/s0012-821X(03)00360-1.

Chatzipetros, A., Kokkalas, S., Pavlides, S., Koukouvelas, I., 2005. Palaeoseismic data and their implication for active deformation in Greece. J. Geodyn. 40, 170-188. doi:10.1016/j.jog.2005.07.005.

Chatzipetros, A., Pavlides, S., Mountrakis, D., 1998. Understanding the 13 May 1995 western Macedonian earthquake: a paleoseismological approach. J. Geodyn. 26, 327-339.

Cianetti, S., Gasparini, P., Boccaletti, M., Giunchi, C., 1997. Reproducing the velocity and stress field in the Aegean region. Geophys. Res. Lett. 24, 2087-2090.

Cianetti, S., Gasparini, P.,Giunchi, C.,Boschi, E., 2001. Numerical modeling of the Aegean-Anatolian region: geodynamic constraints from observed rheological heterogeneities. Geophys. J. Int. 146, 760-780.

Clarke, P. J., 1996. Tectonic motion and tectonic deformation in Greece from GPS measurements. PhD Thesis, University of Oxford, Exeter College, Oxford.

Clarke, P. J., Davies, R.R., England, P.C., Parsons, B., Billiris, H., Paradissis, D., Veis, G., Cross, P.A., Denys, P.H., Ashkenazi, V., Bingley, R., Kahle H.-G., Muller, M.V., Briole, P., 1998. Crustal strain in central Greece from repeated GPS measurements in the interval 1989-1997. Geophys. J. Int. 135, 195-214.

857 Clarke, P. J., Davies, R.R., England, P.C., Parsons, B.E., Billiris, H., Paradissis, D., Veis, G.,
858 Denys, P.H., Cross, P.A., Ashkenazsi,V., Bingley, R., 1997. Geodetic estimate of seismic
859 hazard in the Gulf of Korinthos. Geophys. Res. Lett. 24(11), 1303-1306.
860
861 Cocard, M., Kahle, H.-G., Peter, Y., Geiger, A., Veis, G., Felekis, S., Paradissis, D., Billiris, H.,
862 1999. New constraints on the rapid crustal motion of the Aegean region: recent results
863 inferred from GPS measurements (1993-1998) across the West Hellenic Arc, Greece. Earth
864 Planet. Sci. Lett. 172, 39-47.
865
866 Cross, P., 1992. Working Paper 6: Advanced least squares applied to position fixing, 2nd
867 Edition. School of Surveying. University of East London editions.
868
869 Cruddace, P. R., Cross, P.A., Veis, G., Billiris, H., Paradissis, D., Galanis, J., Lyon-Caen, H.,
870 Briole, P., Ambrosius, B.A.C., Simons, W.J.F., Roegies, E., Parsons, B., England, P., Kahle,
871 H.-G., Cocard, M., Yannick, P., Stavrakakis, G., Clarke, P., Lilje, M., 1999. An
872 interdisciplinary approach to studying seismic hazard throughout Greece. In Geodesy beyond
873 2000: the challenges of the first decade. International Association of Geodesy Symposia 121,
874 279-284.
875
876 Davies, P., 1997. Assembling the IGS polyhedron. A densinfied weekly GPS terrestrial reference
877 frame. PhD Thesis, University of Newcastle Upon Tyne, Newcastle Upon Tyne.
878

879 Davies, P., Blewitt, G., 2000. Methodology for global geodetic time series estimation: A new
880 tool for geodynamics. J. Geophys. Res. 105 (B5), 11,083-11,100.
881
882 Davies, R.R., England, P., Parsons, B., Billiris, H., Paradissis, D., Veis, G., 1997. Geodetic strain
883 in Greece in the interval 1892-1992. J. Geophys. Res. 102(B11), 24,571-24,588.
884
885 Doutsos, T., Piper, D.J.W., 1990. Listric faulting, sedimentation and morphological evolution of
886 the Quaternary eastern Corinth rift, Greece. First stages of continental rifting. Bull. Geol.
887 Soc. Am. 102, 812-829.
888
889 Dow, J. M., Neilan, R.E., Gendt, G., 2005. The International GPS Service: Celebrating the 10th
890 anniversary and looking to the next decade. Advances in Space Research 36, 320-326.
891 doi:10.1016/j.asr.2005.05.125.
892
893 England, P., Molnar, P., 1997. The field of crustal velocity in Asia calculated from Quaternary
894 rates of slip on faults. Geophys. J. Int. 130, 551-582.
895
896 Estey, L., Meertens, C., 1999. TEQC: The Multi-Purpose Toolkit for GPS/GLONASS data. GPS
897 solutions 3(1), 42-49.
898
899 Evangelidis, C.P., Konstantinou, K.I., Melis, N.S., Charalambakis, M., Stavrakakis, G. N., 2008.
900 Waveform relocation and focal mechanism analysis of an earthquake swarm in Trichonis
901 Lake, Western Greece. Bull. Seism. Soc. Am. 98, 804-811. doi: 10.1785/0120070185.

Frank, F. C., 1966. Deduction of earth strains from survey data. Bull. Seismol. Soc. Am. 56(1), 32-42.

Field, E. H., Johnson, D.D., Dolan, J.F., 1999. A mutually consistent seismic-hazard source model for Southern California. Bull. Seism. Soc.Am. 89(3), 559–578.

Gurtner, W., 1994. RINEX: The Receiver Independent Exchange Format. GPS WORLD 5(7), 48-52.

Goldsworthy, M., Jackson, J., 2001. Migration of activity within normal fault systems: examples from the Quaternary of mainland Greece. J. Struct. Geol. 23, 489–506.

Hatzfeld, D., Martinod, J., Bastet, G., Gautier, P., 1997. An analogue experiment for the Aegean to describe the contribution of gravitational potential energy. J. Geophys. Res. 102, 649-659.

Hollenstein, C., Müller, M.D., Geiger, A., Kahle, H.-G., 2008. Crustal motion and deformation in Greece from a decade of GPS measurements, 1993-2003. Tectonophysics 449. doi:10.1016/j.tecto.2007.12.006.

Holt, W. E., Haines. J., 1993. Velocity fields in deforming Asia from the inversion of earthquake-released strains. Tectonics 12(1), 1-20.

Jackson, J., 1994. Active Tectonics of the Aegean Region. Ann. Rev. Earth. Planet. Sci. 22, 239-271.

Jackson, J., McKenzie, D.P., 1988. Rates of active deformation in the Aegean Sea and surrounding regions. Basin Research 1, 121-128.

Jackson, J., McKenzie D.P., 1988a. The relationship between plate motions and seismic moment tensors, and the rates of active deformation in the Mediterranean and Middle East. Geophys. J. R. Astr. Soc. 93, 45-73.

Jenny, S., Saskia, G., Giardini, D., Kahle, H.-G., 2004. Earthquake recurrence parameters from seismic and geodetic strain rates in the eastern Mediterranean. Geophys, J. Int. 157, 1331-1347. doi:10.1111/j.1365-246X.2004.02261.x.

Jones, C. H., Unruh, J.R., Sonder L.J.,1996. The role of gravitational potential energy in active deformation in the southwestern United states. Nature 381, 37-41.

Kahle, H.-G., Cocard, M., Peter, Y., Geiger, A., Reilinger, R., Barka, A., Veis, G., 2000. GPS-derived strain rate field within the boundary zones of the Eurasian, African, and Arabian Plates. J. Geophys. Res. 105(B10), 23,353-23,370.

947 Kahle, H.-G., Cocard, M., Peter, Y., Geiger, A., Reilinger, R., McClusky, S., King, R., Barka,
948 A., Veis, G., 1999. The GPS strain rate field in the Aegean Sea and western Anatolia.
949 Geophys. Res. Lett. 26(16), 2513-2516.
950
951 Kahle, H.-G., Straub, C., Reilinger, R., McClusky, S., King, R., Hurst, K., George Veis, G.,
952 Kastens, K., Cross, P., 1998. The strain rate field in the eastern Mediterranean region
953 estimated by repeated GPS measurements. Tectonophysics 294, 237-252.
954
955 Kahle, H.-G., Muller, M.V., Veis, G., 1996., Trajectories of crustal deformation of western
956 Greece from GPS observations 1989-1994. Geophys. Res. Lett. 23(16), 677-680.
957
958 Kahle, H.-G., Müller M.V., Geiger, A., Danuser, G., Mueller, S., Veis, G., Billiris, H., Paradissis,
959 D., 1995. The strain field in northwestern Greece and the Ionian islands: results inferred from
960 GPS measurements. Tectonophysics 249, 41-52.
961
962 Kanamori, H., 1977. The energy release in great earthquakes. J. Geophys. Res. 82, 2981-2987.
963
964 Kokkalas, S., Pavlides, S., Koukouvelas, I., Ganas, A., Stamatopoulos, L., 2007. Paleoseismicity
965 of the Kaparelli fault (eastern Corinth Gulf): evidence for earthquake recurrence and fault
966 behavior. Boll. Soc. Geol. It (Ital.J.Geosci) 126, 387-395.
967
968 Kokkalas, S.,Doutsos, T., 2001. Strain-dependent stress field and plate motions in the south-east
969 Aegean region. J. Geodyn, 32, 311-332.

Konstantinou, K.I., Melis, N.S., Lee, S-J., Evangelidis, C.P., Boukouras, K., 2009. Rapture process and aftreshocks relocation of the 8 June 2008 (Mw 6.4) earthquake in NW Peloponnese, western Greece. Bull. Seism. Soc. Am. 99, 3374-3389. doi:10.1785/0120080301.

Koukouvelas, I., Stamatopoulos, L., Katsonopoulou, D., Pavlides, S., 2001. A palaeoseismological and geoarchaeological investigation of the Eliki fault, Gulf of Corinth, Greece. J. Struct. Geol. 23, 531–543.

Kreemer, C., Holt, W.E., Goes, S., Govers, R., 2000. Active deformation in eastern Indonesia and the Philippines from GPS and seismic data. J.Geophys.Res (B1). 105, 663-680.

Kostrov, B., 1974. Seismic moment and energy of earthquakes and seismic flow of rock. Izv.Acad.Sci.USSR Phys. Solid Earth 97, 23-44.

Lavallée, D.A., 2000. Tectonic plate motions from global GPS measurements. PhD Thesis. University of Newcastle Upon Tyne, Newcastle Upon Tyne.

Latorre, D., Virieux, J., Monfret, T., Monteiller, V., Vanorio, T., Got, J-L., Lyon-Caen, H., 2004. A new seismic tomography of Aigion area (Gulf of Corinth, Greece) from the 1991 data set. Geophys. J.Int. 159, 1013-1031. doi:10.1111/j.1365-246X.2004.02412.x.

994 Leeder, M.R., Portman, C., Andrews, J.E., Collier, R.E.RI., Finch, E., Gawthorpe, R.L.,
995 McNeill, L.C., Pérez-Arlucea, M., Rowe, P., 2005. Normal faulting and crustal deformation,
996 Alkyonides Gulf and Perachora peninsula, eastern Gulf of Corinth rift, Greece. J Geol. Soc.
997 London 162, 549-561. doi:10.1144/0016-764904-075.
998
999 Le Pichon, X., Angelier, J., 1979. The Hellenic arc and trench system: a key to the evolution of
1000 eastern Mediterranean. Tectonophysics 60, 1-42.
1001
1002 Le Pichon, X., Chamot-Rooke, N., Lallemant, S., 1995. Geodetic determination of the
1003 kinematics of central Greece with respect to Europe: Implications for eastern Mediterranean
1004 tectonics. J. Geophys. Res. 100(B7), 12,675-12,690.
1005
1006 Lundgren, P., Giardini, D., Russo, R., 1998. A geodynamic framework for eastern Mediterranean
1007 kinematics. Geophys.Res. Lett. 25, 4007-4010.
1008
1009 Lyon-Caen, H., Papadimitriou, P., Deschamps, A., Bernard, P., Makropoulos, K., Pacchiani, F.,
1010 Patau, G., 2004. First results of the CRLN seismic network in the western Corinth Rift:
1011 evidence for old-fault reactivation. C.R. Geosci, 336, 343-351.
1012 doi:10.1016/j.crte.2003.12.004.
1013
1014 Mantovani, E., Viti, M., Albarello, D., Tamburelli, C., Babbucci, D., Cenni, N., 2000. Role of
1015 kinematically induced horizontal forces in Mediterranean tectonics: insight from numerical
1016 modeling. J. Geodyn. 30, 287-320.

Martinod, J., Hatzfeld, D., Brun, J-P., Gautier, P., 2000. Continental collision, gravity spreading and kinematics of Aegean and Anatolia. Tectonics 19 (2), 290-299.

Masson, F., Chéry, J., Hatzfeld, D., Martinod, J., Vernant, P., Tavakoli, F., Ghafory-Ashtiani, M., 2005. Seismic versus aseismic deformation in Iran inferred from earthquakes and geodetic data. Geophys. J.Int. 160, 217-226. doi:10.1111/j.1365-246X.2004.02465.x.

McClusky, S., Balassanian, S., Barka, A., Demir, C., Ergintav, S., Georgiev, I., Gurkan, O., Hamburger, M., Hurst, K., Kahle, H., Kastens, K., Kekelidze, G., King, R., Kotzev, V., Lenk, O., Mahmoud, S., Mishin, A., Nadariya, M., Ouzounis, A., Paradissis, D., Peter, Y., Prilepin, M., Reilinger, R., Sanli, I., Seeger, H., Tealeb, A., Toksoz, M.N., Veis, G., 2000, Global Positioning System Constraints on plate kinematics and dynamics in the eastren Mediterranean and Caucasus. J. Geophys. Res. 105(B3), 5695-5719.

McKenzie, D.P., 1978. Active tectonics of the Alpine-Himalayan Belt: the Aegean Sea and surrounding regions. Geophys. J. R. Astr. Soc. 55, 217-254.

McKenzie, D.P., 1972. Active tectonics of the Mediterranean Region. Geophys. J. R. Astr. Soc. 30, 109-185.

Meyer, B., Armijo, R., De Chabalier, J., Delacourt, C., Ruegg, J., Acache, J., Brioke, P., Papanastasiou, D., 1996. The 1995 Grevena (Northern Greece) earthquake: fault model

constrained with tectonic observations and SAR interferometry. Geophys. Res. Lett. 23, 2677-2680.

Meijer , P.T., Wortel, M.J.R., 1997. Present-day dynamics of the Aegean region: a model analysis of the horizontal pattern of stress and deformation. Tectonics 16 (6), 879-895.

Moretti, I., Sakellariou, D., Lykousis, V., Micarelli, L., 2003. The Gulf of Corinth : an active half graben?. J. Geodyn. 36, 323-340.

Niell, A.E., 1996. Global mapping functions or the atmosphere delay at radio wavelengths. J. Geophys. Res. 101(B2), 3227-3246.

Nyst, M.C.J., Thatcher, W., 2004. New constraints on the active tectonic deformation of the Aegean. J.Geophys.Res. 109, B11406. doi:11410.11029/12003JB002830.

Pancha, A., Anderson, J., Kreemer, C., 2006. Comparison of Seismic and Geodetic Scalar Moment Rates across the Basin and Range Province. Bull. Seism. Soc. Am. 96, 11-32. doi:10.1785/0120040166.

Pantosti, D., De Martini, P.M., Koukouvelas, I., Stamatopoulos, L., Palyvos, N., Pucci, S., Lemeille, F., Pavlides, S., 2004. Palaeoseismological investigations of the Aigion Fault (Gulf of Corinth, Greece). C.R. Geosci, 336, 335-342. doi:10.1016/j.crte.2003.12.005.

1063 Pantosti, D., Collier, R., D' Addezio, G., Masana, E., Sakellariou, D., 1996. Direct geological
1064 evidence for prior earthquakes on the 1981 Corinth fault (Central Greece). Geophys. Res.
1065 Lett. 23, 3795-3798.
1066
1067 Papadimitriou, E. E., Sykes, L. R., 2001. Evolution of the stress field in the northern Aegean Sea
1068 (Greece). Geophys. J. Int. 146, 747-759.
1069
1070 Papazachos, B.C., 1990, Seismicity of the Aegean and the surrounding area. Tectonophysics
1071 178, 287-308.
1072
1073 Papazachos, B.C., Papaioannou, C., Papazachos, C.B., Savvaidis, S.A., 1999. Rupture zones in
1074 the Aegean region. Tectonophysics 308, 205-221.
1075
1076 Papazachos, B.C., and Papazachou (1997). The earthquakes of Greece, Ziti Editions,
1077 Thessaloniki.
1078
1079 Papazachos, C. B., Kiratzi, A., 1996. A detailed study of the active crustal deformation in the
1080 Aegean and surrounding area. Tectonophysics 253, 129-153.
1081
1082 Pavlides, S.B., Caputo, R., 2004. Magnitude versus faults' surface parameters: quantitative
1083 relationships from the Aegean Region. Tectonophysics 380, 159-188.
1084 doi:10.1016/j.tecto.2003.09.019.
1085

1086 Pavlides, S.B., King, G.C.P., 1998. The 1995 Kozani-Grevena earthquake (N. Greece): an
1087 introduction. J. Geodyn. 26, 171-173.
1088
1089 Pavlides, S.B., Zouros, N.C., Chatzipetros, A.A., Kostopoulos, D.S., Mountrakis, D.M., 1995.
1090 The 13 May 1995 western Macedonia, Greece (Kozani-Grevena) earthquake; preliminary
1091 results. Terra Nova 7, 544-549.
1092
1093 Peter, J.D., Kahle, H.-G., Cocard, M., Veis, G., Felekis, S., Paradissis, D., 1998. Establishment
1094 of continuous GPS network across Kephalonia Fault Zone, Ionian islands, Greece.
1095 Tectonophysics 294, 253-260.
1096
1097 Plag, H.-P., Ambrosius, B., Baker, T. F., Beutler, G., Bianco, G., Blewitt, G., Boucher, C.,
1098 Davis, J. L., Degnan, J. J., Johansson, J. M., Kahle, H.-G., Kumkova, I., Marson, I., Mueller,
1099 S., Pavlis, E. C., Pearlman, M. R., Richter, B., Spakman, W., Tatevian, S. K., Tomasi, P.,
1100 Wilson, P., Zerbini, S., 1998. Scientific objectives of current and future WEGENER
1101 activities. Tectonophysics 294, 177-223.
1102
1103 Prescott, W., 1976. An extension of Frank's method for obtaining crustal shear strains from
1104 survey data. Bull.Seism.Soc. Am 66,1847-1853.
1105
1106 Reilinger, R., McClusky, S.C., Oral, M.B., King, R.W., Toksoz, M.N., Barka, A.A., Kinik, I.,
1107 Lenk, O., Sanli, I., 1997. Global Positioning System measurements of present-day crustal

movements in the Arabia-Africa-Eurasia plate collision zone. J. Geophys. Res. 102(B5), 9983-9999.

Rigo, A., Lyon-Caen, H., Armijo, R., Deschamps, A., Hatzfeld, D., Makropoulos, K., Papadimitriou, P., Kassaras, I., 1996. A microseismic study in the Gulf of Corinth (Greece): Implications for large-scale normal faulting mechanisms. Geophys. J. Int. 126, 663-688.

Roberts, S., Koukouvelas, I., 1996. Structural and seismological segmentation of the Gulf of Corinth fault system: implications for models of fault growth. Ann. Geophys. 23, 619-646.

Rontogianni, S., 2007. Strain rates in Greece using GPS measurements from 1994-2000. PhD Thesis. University of Newcastle Upon Tyne, Newcastle Upon Tyne.

Savage, J.C., Lisowski, M., 1998. Viscoelastic coupling model of the San Andreas Fault along the big bend, southern California. J. Geophys. Res. 103 (B4), 7281-7292.

Shen-Tu, B., Holt, W. E., Haines, A.J., 1998. Contemporary kinematics of the Western United states determined from earthquake moment tensors, very long base interferometry, and GPS observations, J. Geophys. Res. 103(B8), 18,087-18,117.

Smith, W.H.F., Wessel, P., 1990. Gridding with continuous curvature spines in tension. Geophysics 55, 293-305.

SOPAC Scripps Orbit and Permanent Array Center, 2006. web page: http://sopac.ucsd.edu/dataArchive/ .

Stiros, S. C., 1993. Kinematics and deformation of central and southwestern Greece from historical triangulation data and implications for the active tectonics of the Aegean, Tectonophysics 220, 283-300.

Straub, C., Kahle, H.-G., 1997. GPS and geologic estimates of the tectonic activity in the Marmara Sea region, NW Anatolia. J. Geophys. Res. 102(B12), 27,587-27,601.

Taymaz, T., Jackson, J., McKenzie D.P., 1991. Active tectonics of the north and central Aegean Sea. Geophys. J. Int. 106, 433-490.

Theodulidis, N., Lekidis, V., Margaris, B., Papazachos, C.B., Papaioannou, C., Dimitriu, P., 1998. Seismic Hazard assessment and design spectra for the Kozani-Grevena region (Greece) after the earthquake of May 13, 1995. J. Geodyn. 26, 375-391.

UNAVCO, TEQC - tutorial, 2006 .
webpage: http://facility.unavco.org/software/teqc/teqc.html .

Ward, S.N., 1998a. On the consistency of earthquake moment rates, geological fault data, and space geodetic strain: the United States. Geophys. J. Int. 134, 172–186.

Ward, S.N., 1998b. On the consistency of earthquake moment release and space geodetic strain rates: Europe. Geophys. J. Int. 135, 1011–1018.

Welsch, W.M., 1983. Finite element analysis of strain patterns from geodetic observations across a plate margin. Tectonophysics 97, 57-71.

Figure 1. Major tectonic faults and location map of Greece (Papazachos and Papazachou, 1997).

Figure 2. GPS networks in Greece used in this study.

Figure 3. The 43 Global GPS sites used in the processing stage.

Figure 4. Local sites histogram showing the interval in months between the first, and the last occupation as described in Table 3.

Figure 5. Scatter plot showing the east, and north velocity errors in mm/yr relative to the data span from the first to the last occupation in months.

Figure 6. Velocities for the Greek sites in a Eurasian Fixed reference frame from the period 1994-2000 as formed in this study. Residuals to the European Euler pole with 39% confidence error ellipses. Errors have scaled by the unit variance. The velocities arrows and error ellipses in black describe sites with more than 22 months observation span. The blue velocity arrows and error ellipses describe the sites with more than 16 and up to 22 months data span. The green velocity arrows and error ellipses describe sites with less than 16 months data span. For the sites in green color the error ellipses have been multiplied, for viewing purposes, by a factor of 0.3.

Figure 7. Principal strain rates computed for the 22 polygonal regions. Extensional axes are shown as thick lines and compressional axes as shown as thin lines. Results are given in ppm/yr. The grey arrows show station residuals to the uniform strain (most sites form part of more than one neighboring polygon).

Figure 8. Geodetic rigid-body rotation rates computed from the polygonal regions (degrees/Myr). Uncertainties (1-sigma) are shown in grey. Strong clockwise rotation is observed around the North Eastern Aegean, Gulf of Corinth, and Gulf of Evia, with smaller rates around the Grevena and Chalkidiki areas. The sense of rotation changes in the South Aegean and Cyclades area where anti-clockwise rotation is present.

Figure 9. Principal strain rates (left) and rotation rates (right) computed from the minimum curvature grid method.

Figure 10. Comparison of principal geodetic strain rates computed via the two methods described: (left) polygon method, (right) minimum curvature surface method.

Figure 11. (1) Locations of earthquakes taken from the 30 year Harvard CMT catalogue (open triangles). Data are from 1976-2006 with $M_S \geq 4$ and depth $h \leq 40$ km. (2) Earthquake locations taken from the Ambraseys and Jackson (1990) catalogue (open circles) . Data cover the period from 1890 until 1988. The catalogue is focused on central Greece and includes events with $M_S \geq 5.8$. (3) Earthquake locations from the Ambraseys and Jackson (1997) catalogue. Data from 1694 - 1995 focusing on the Gulf of Corinth for $M_S \geq 6$ and depth $h \leq 40$ km (filled triangles).

Figure 12. Seismic strain rate (white arrows) results from seismic catalogues compared to principal geodetic strain (black arrows) for both thicknesses of seismogenic layer: (left) 10 km thickness, right 15 km thickness; (a) 30-year catalogue (b) 100-year catalogue, (c) 300-year catalogue.

Figure 13. Calculated directions of no length change (nlc) from the continuous velocity field (black symbols) compared with fault plane strikes from the combination of all three seismic catalogues (red symbols). Inset map shows earthquake locations and catalogue used: 30-year (red, $M_S \geq 5.5$ only), 100-year (blue), 300-year (green) points.

Figure 14. Earthquake locations with $Mw \geq 5.0$ taken from Harvard CMT catalogue for the period 2000-2008.

Figure1

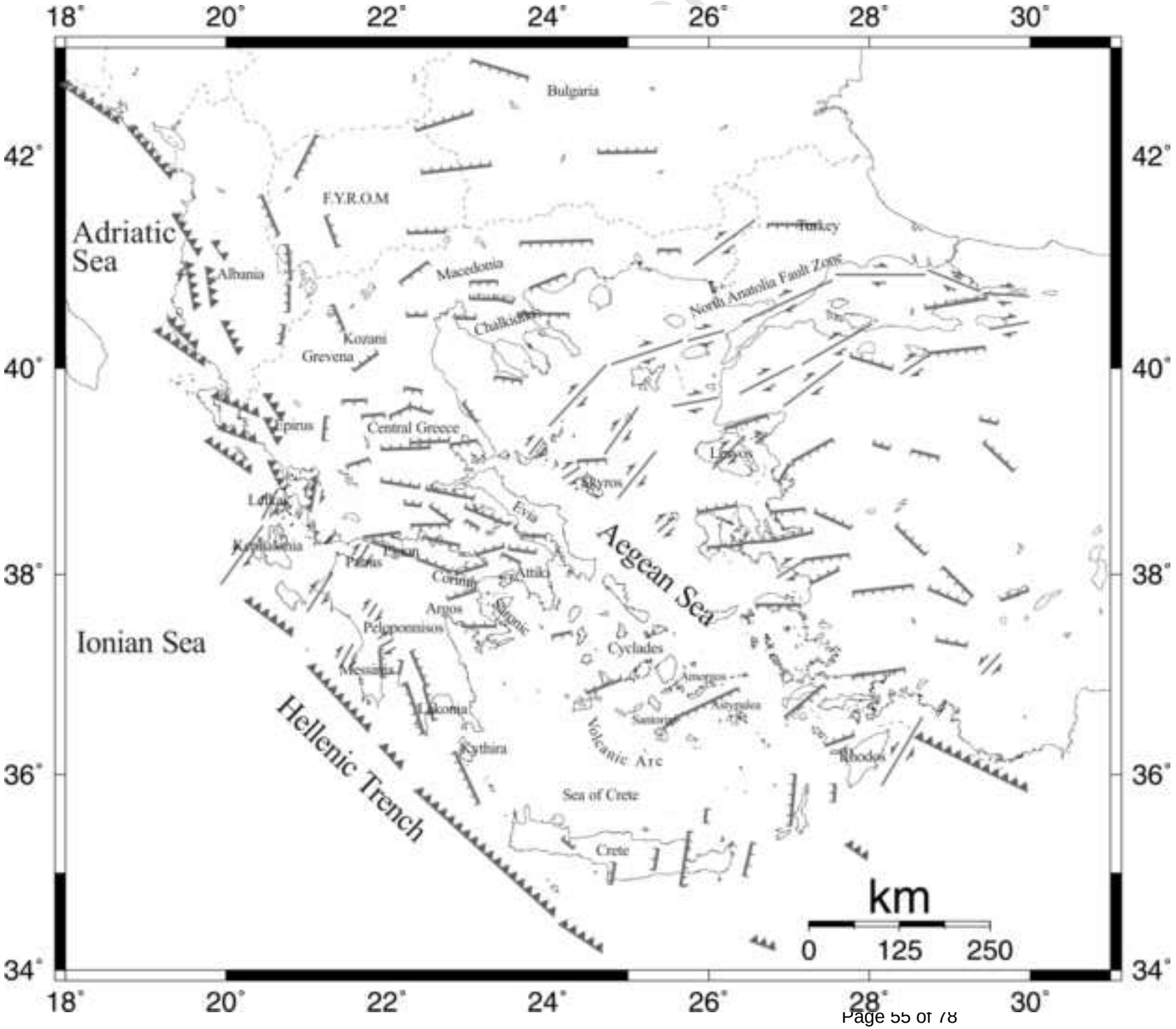
18°
20°
22°
24°
26°
28°
30°
42°
40°
38°
36°
34°
Bulgaria
F.Y.R.O.M
Albania
Macedonia
Turkey
North Anatolia Fault Zone
Adriatic Sea
Kozani
Grevena
Chalkidiki
Epirus
Central Greece
Lesvos
Skyros
Evia
Aegean Sea
Attiki
Argos
Peloponnisos
Ionian Sea
Cyclades
Amorgos
Santorini
Kythira
Volcanic Arc
Rhodos
Sea of Crete
Crete
Hellenic Trench
km
0
125
250

Figure2

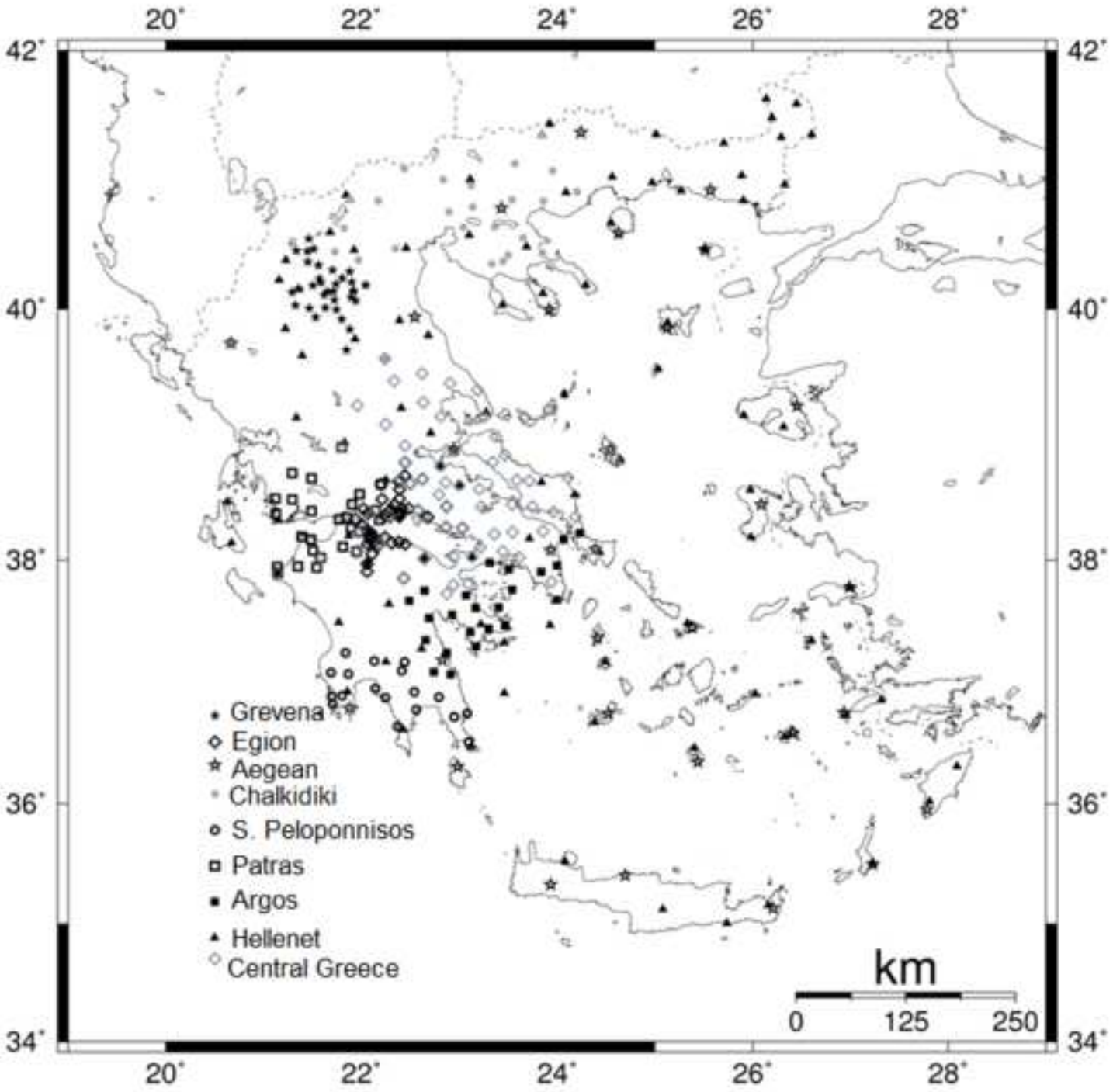
20°
22°
24°
26°
28°
42°
40°
38°
36°
34°
Grevena
Egion
Aegean
Chalkidiki
S. Peloponnisos
Patras
Argos
Hellenet
Central Greece
km
0
125
250

Figure3

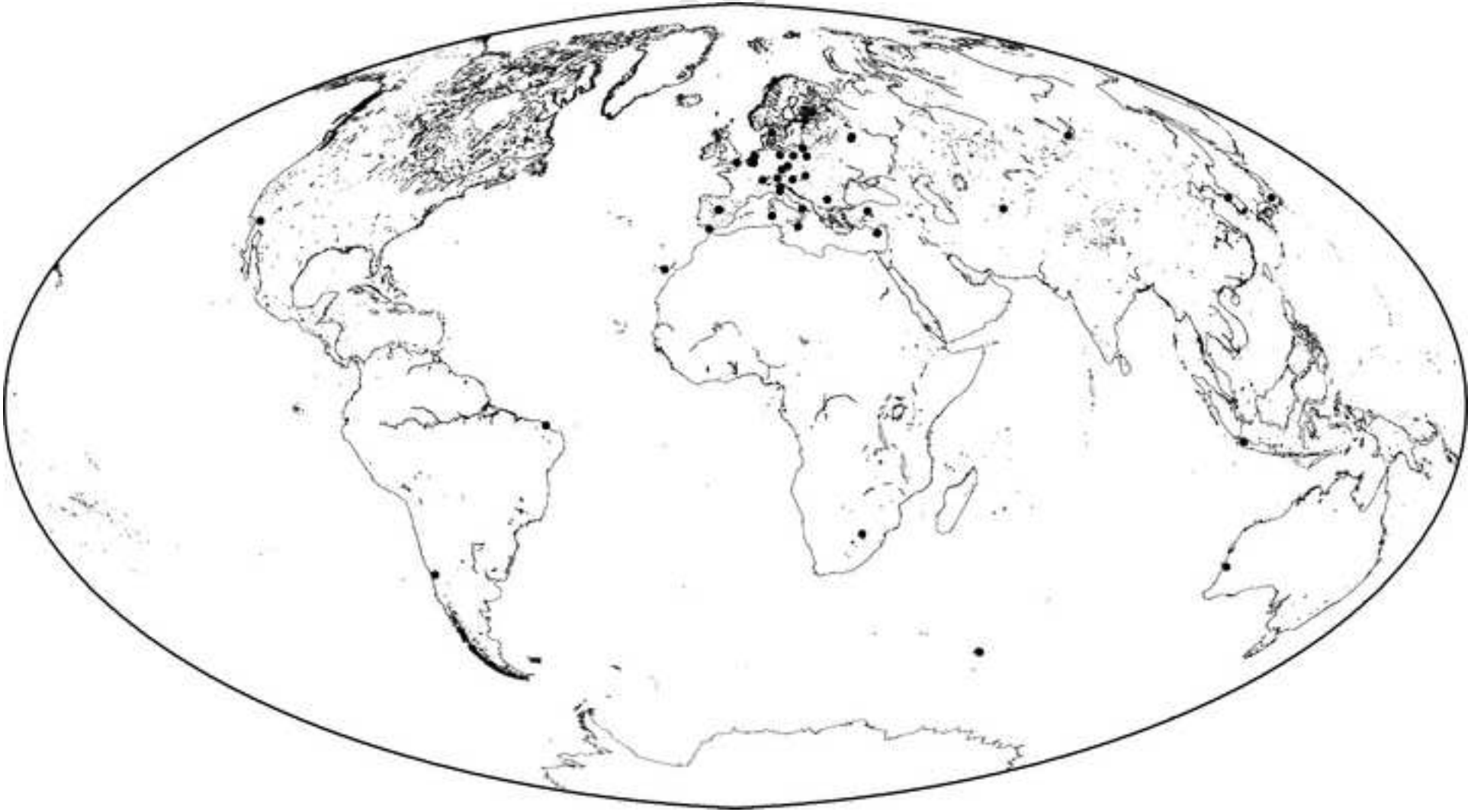

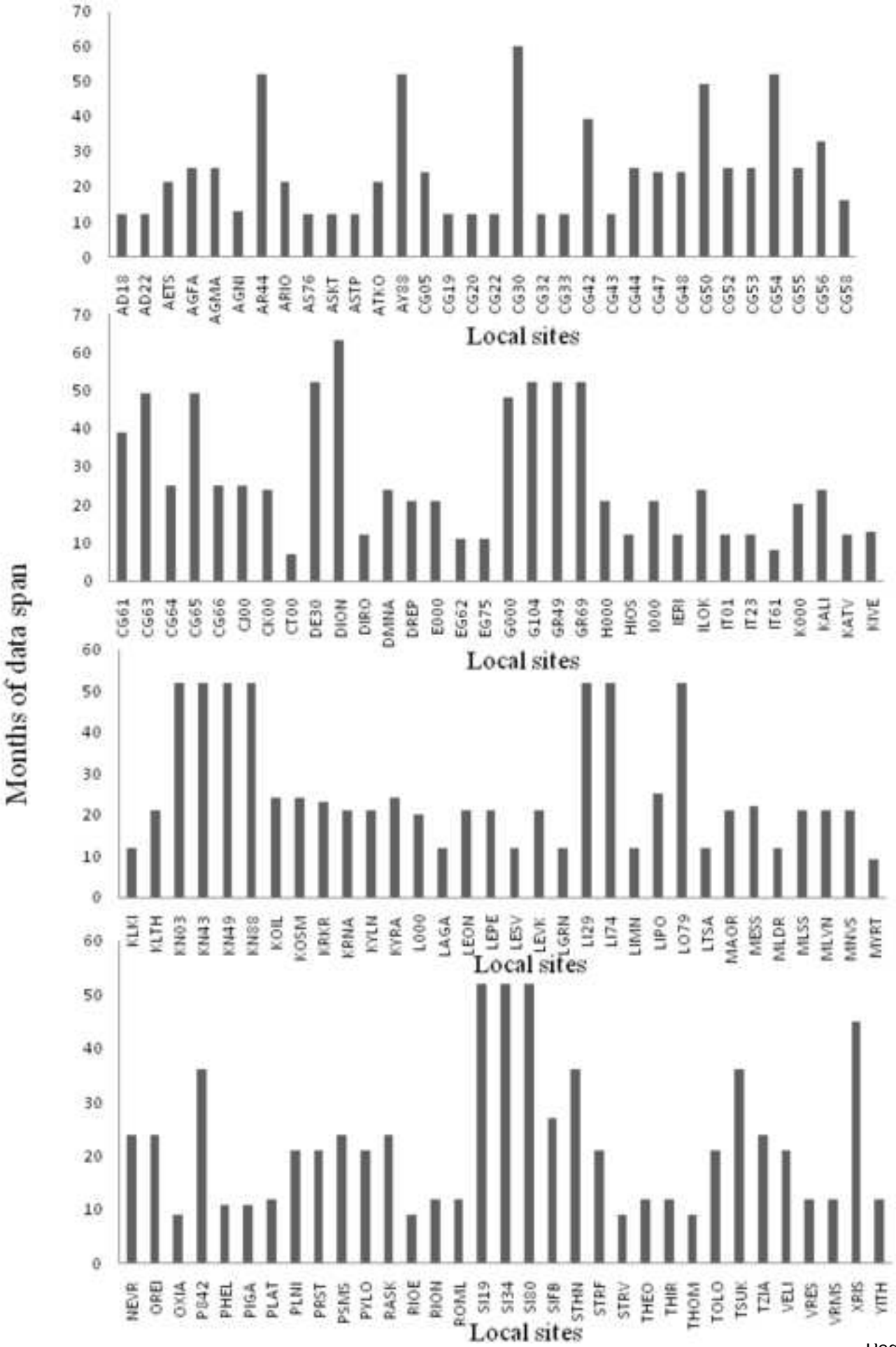

Figure5

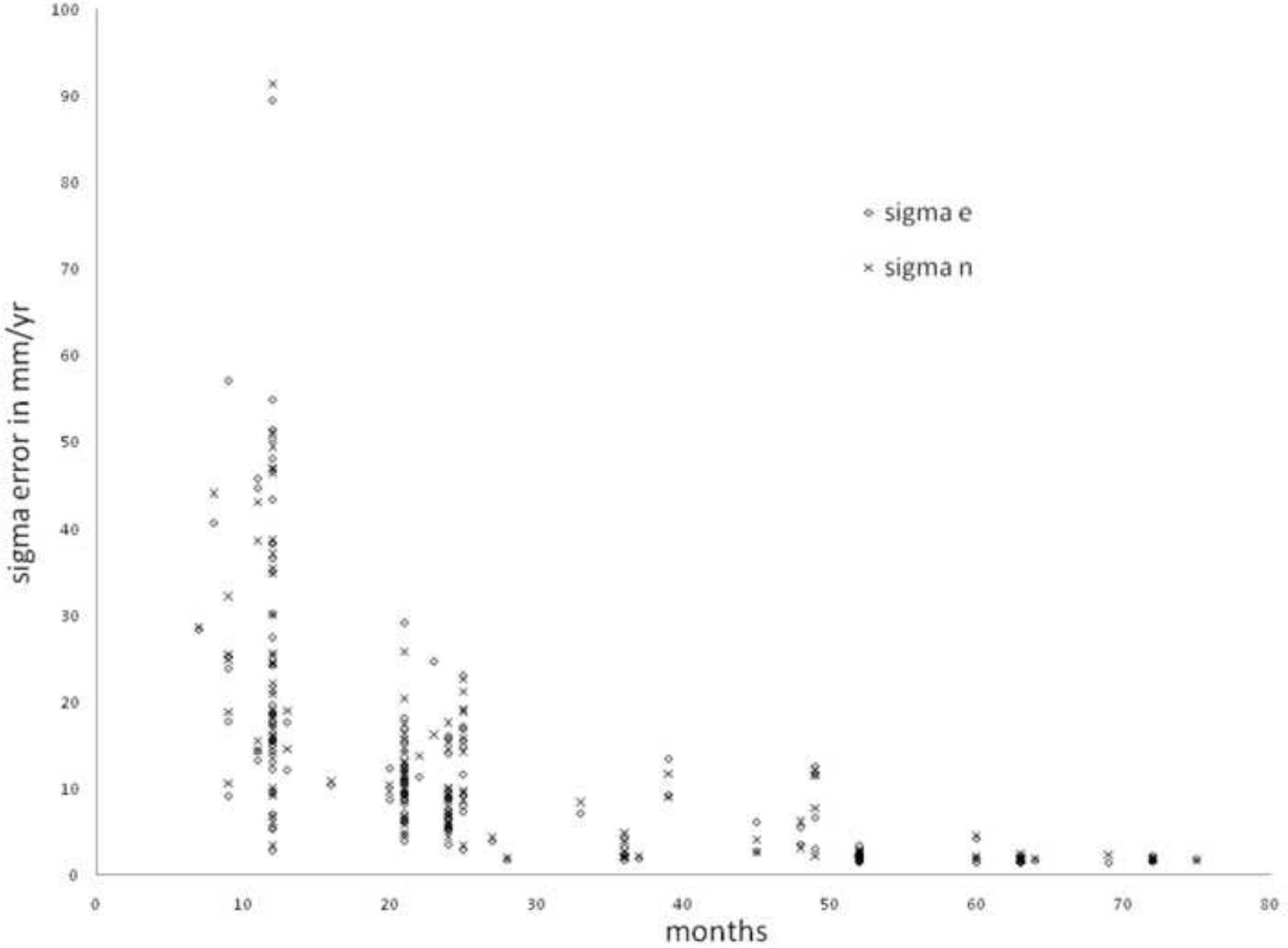
sigma e
sigma n
sigma error in mm/yr
months
0
10
20
30
40
50
60
70
80
90
100

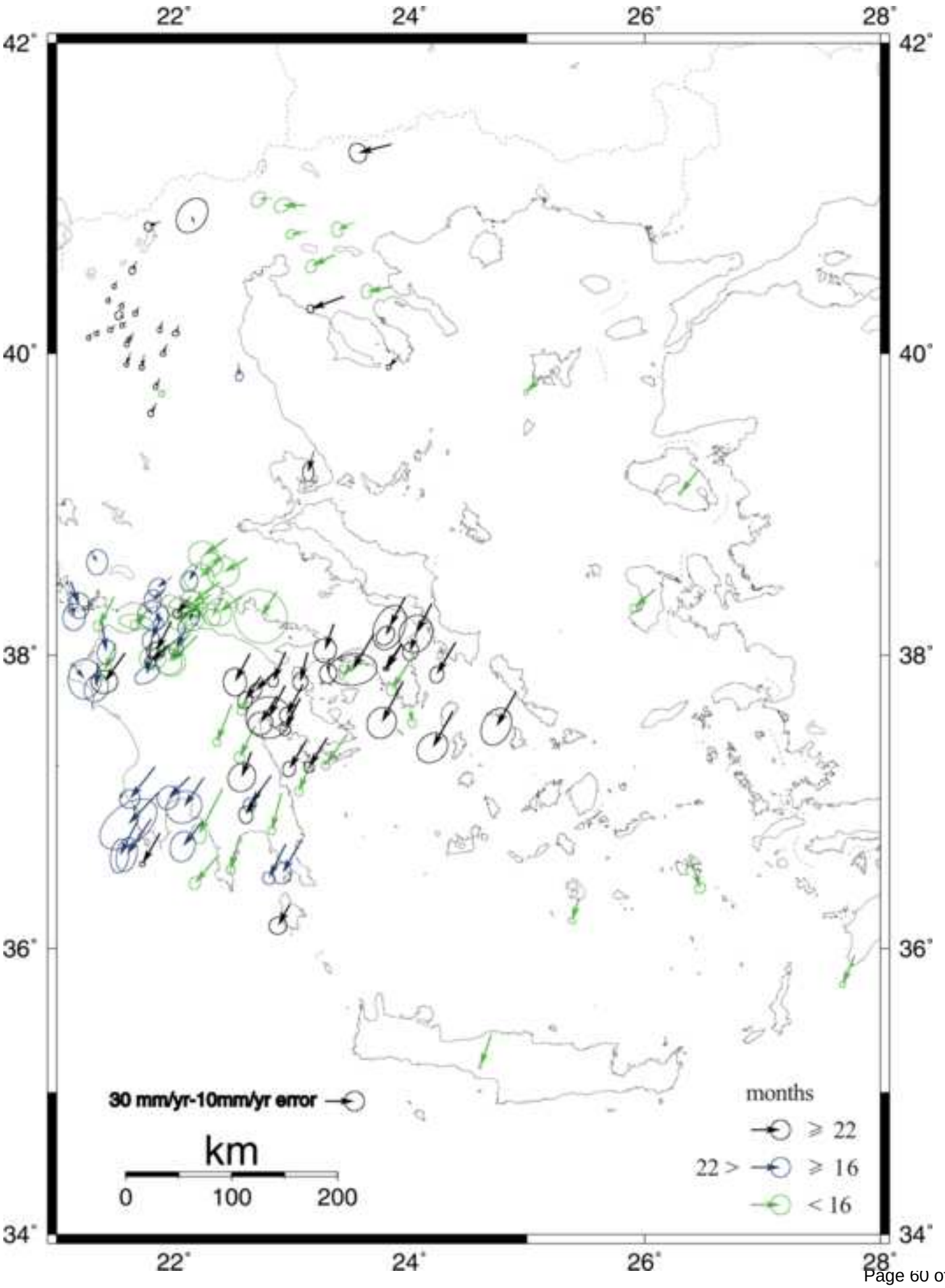

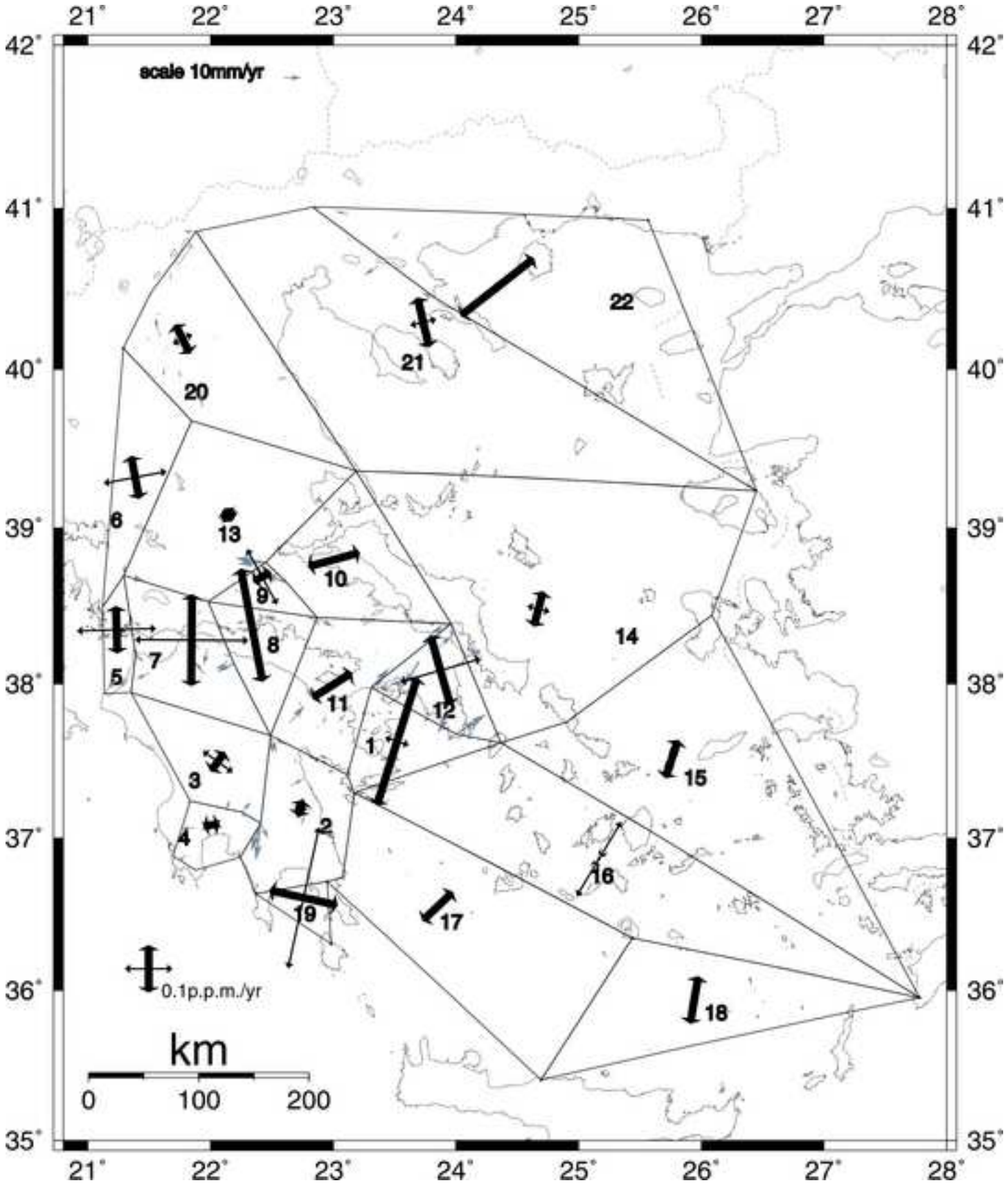

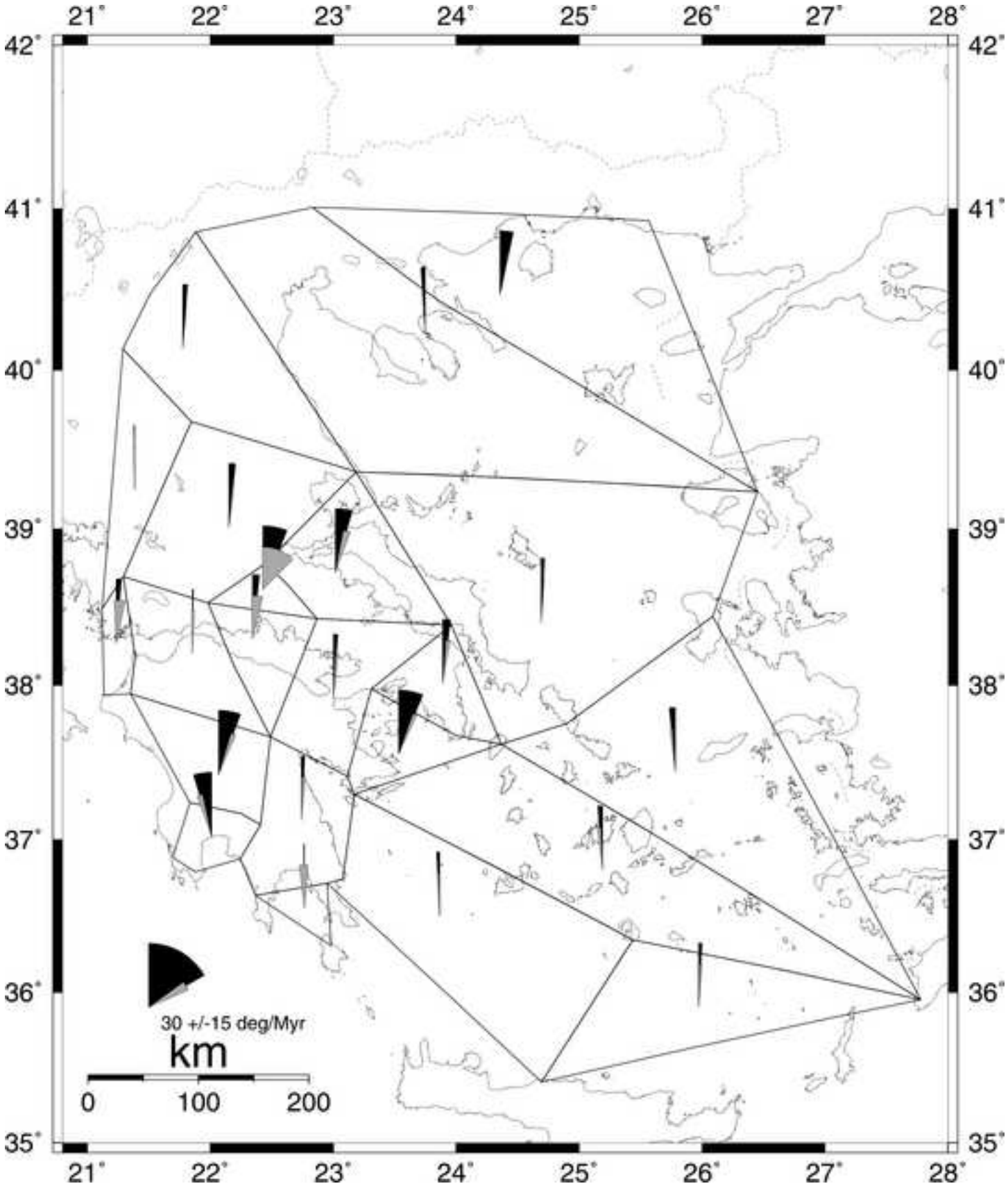

Figure9

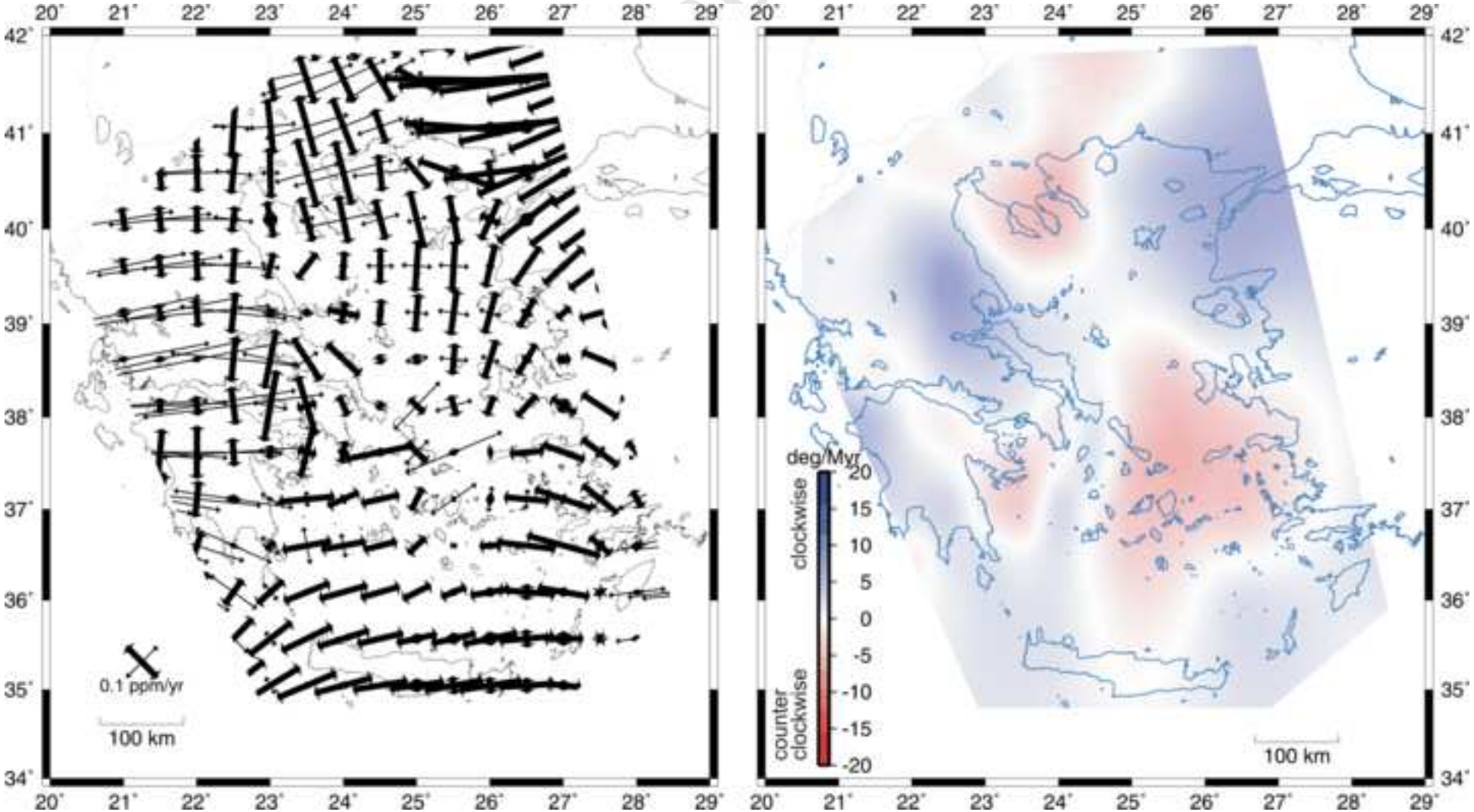
20° 21° 22° 23° 24° 25° 26° 27° 28° 29°
42° 41° 40° 39° 38° 37° 36° 35° 34°
0.1 ppm/yr
100 km
deg/Myr
clockwise
counter clockwise
20 15 10 5 0 -5 -10 -15 -20
100 km

Figure10

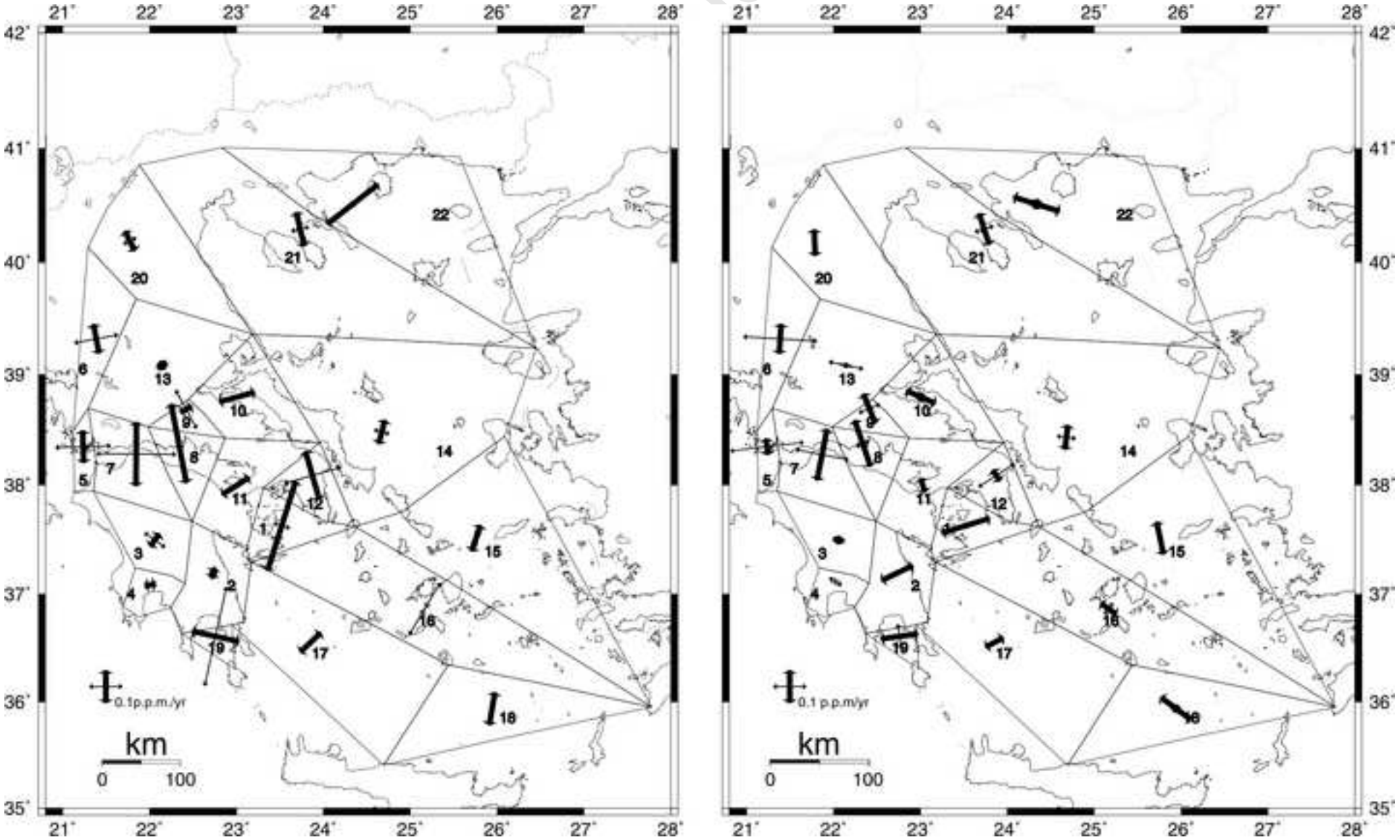
21° 22° 23° 24° 25° 26° 27° 28°
42° 41° 40° 39° 38° 37° 36° 35°
0.1p.p.m./yr
km
0 100
0.1 p.p.m/yr
km
0 100

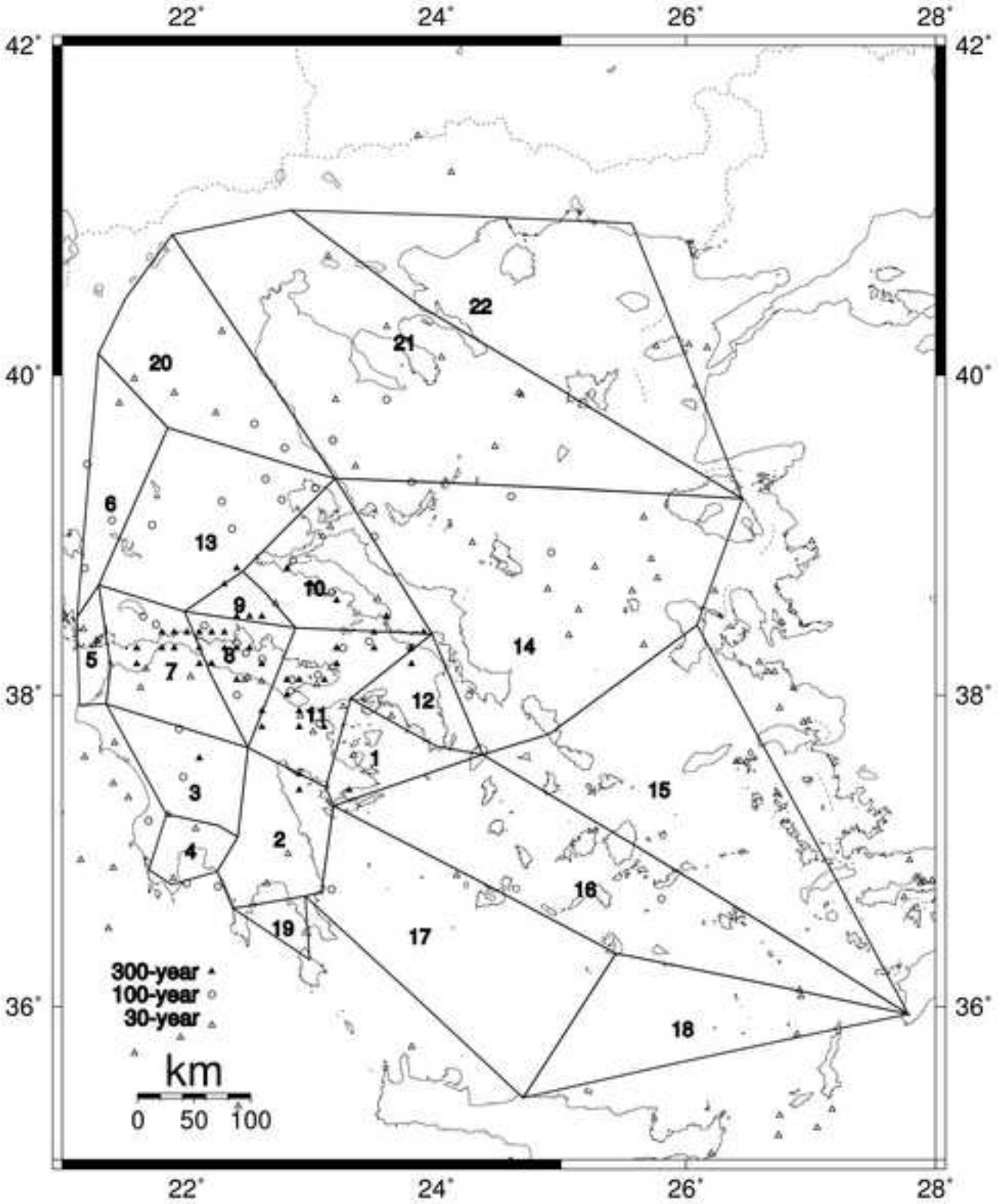

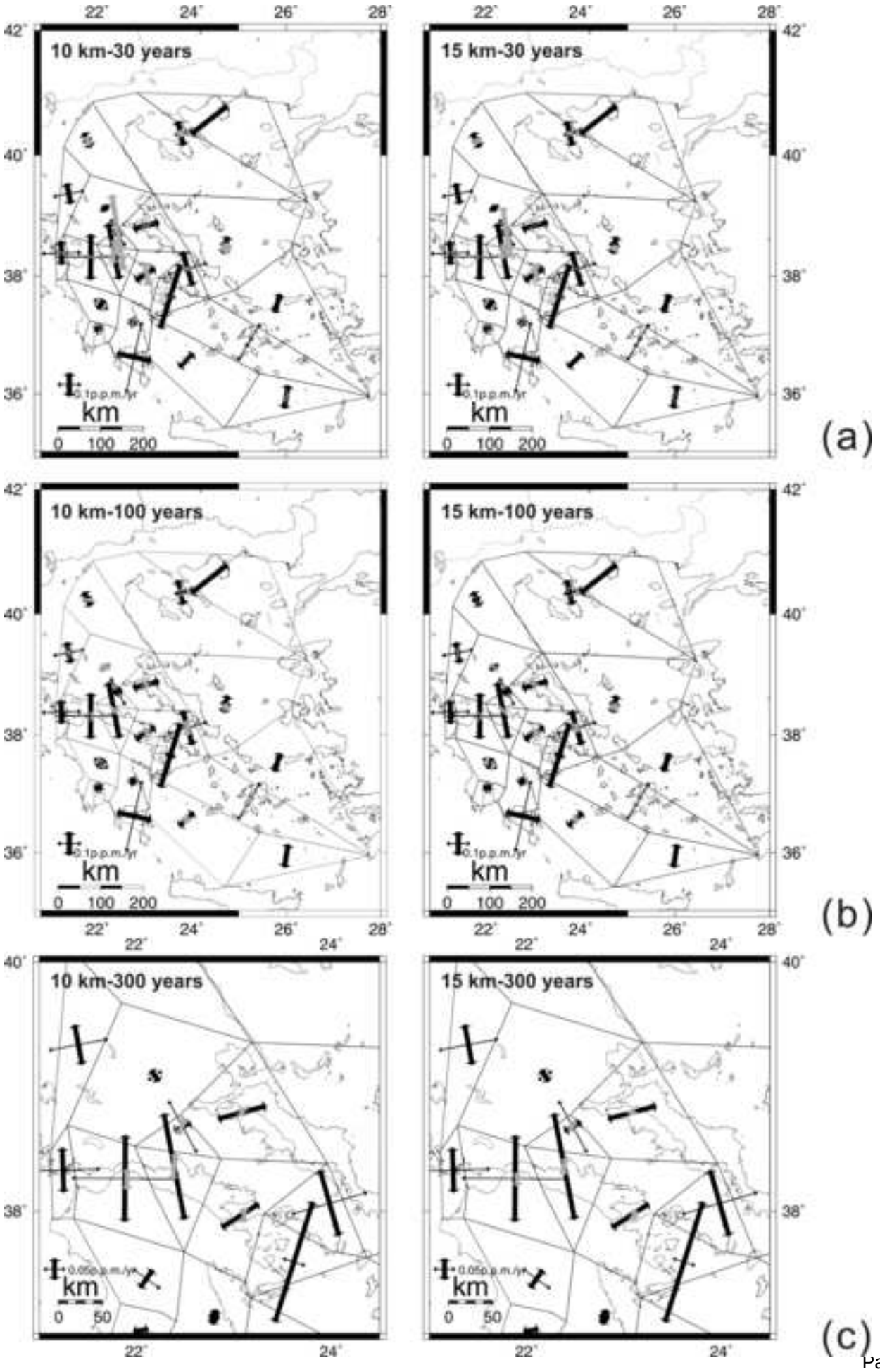

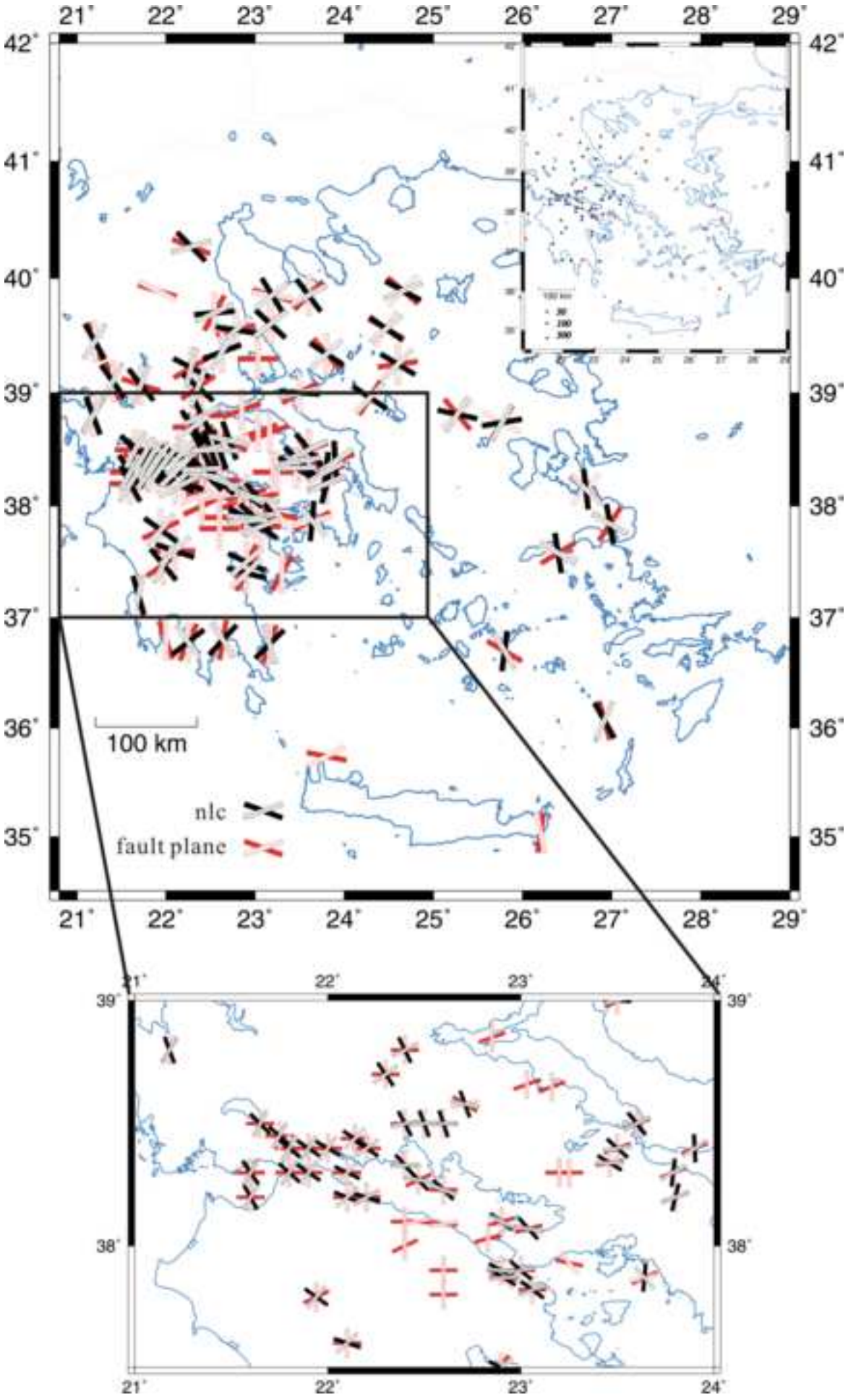

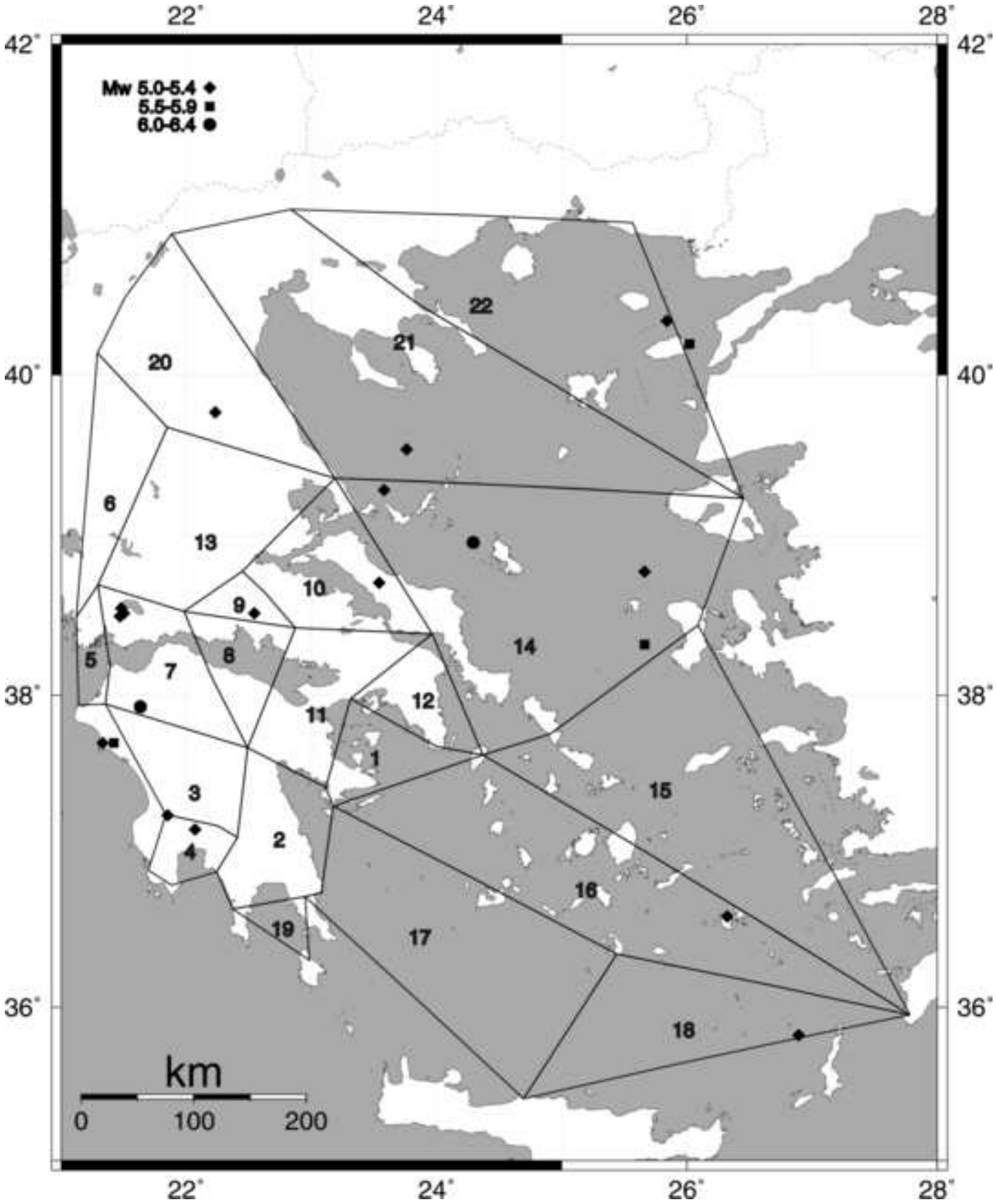

Table 1. GPS campaign data used during the project.

Network	Region	Campaign code	Year	Days of year (DOY)	Local sites
Aegean	Aegean	Aegean94	1994	255-272	4
Aegean	Aegean	Aegean96	1996	252-271	4
SING	Argos	Argos98	1998	179-198	48
SING	Patras	Patra98	1998	284-297	28
SING	Chalkidiki,	Chasp98	1998	263-275	50
SING	Attiki – central Greece	Attiki99	1999	276-285	12
SING	Argos, Patras,	Paspar99	1999	152-163	54
SING	Chalkidiki	Chalk99	1999	283-295	36
SING	Argos, Patras	Argpa00	2000	184-189	32
SING	Chalkidiki	Chalk00	2000	272-276	30
SING	Corinth	Corinth00	2000	091-195	19
Grevena	Grevena	Grev96	1996	128-160	41
Grevena	Grevena	Grev98	1998	153-178	59
Grevena	Grevena	Grev00	2000	245-254	55
Hellenet	Hellenet	Hell97	1997	252-274	72
Egion	Egion	Egion95a	1995	171-176	40
Egion	Egion	Egion95b	1995	276-281	56
Egion	Egion	Egion96	1996	135-153	60
TOTAL					280

Table 2. Processing strategy followed during the project.

Session choice	Strict 24-hour window
Baseline choice	Minimise total baseline length and antenna mismatches, whilst maximising common observation times.
Orbits	IGS precise orbits, held fixed.
Data windowing	10° elevation mask (unless higher in raw data).
Ionosphere model	Ionosphere free observable used; CODE global ionosphere map used to aid ambiguity resolution in wide-lane solutions.
Troposphere model	Saastamoinen model for dry zenith delay using standard atmospheric conditions; wet zenith delay estimated at 2-hour intervals. Niell mapping function (*Niell*, 1996) (wet and dry).
Tidal loading	IERS 1996 Conventions for solid Earth tides incorporated within software. Ocean tide loading specified a priori for 11 major constituents using the CSR4.0 ocean tide model, computed using http://www.oso.chalmers.se/~loading/
Ambiguity resolution	Double-difference ambiguities resolved on per-baseline basis within daily network solutions, using either "Quasi Ionosphere Free" model (campaigns Grevena 96, Patras 98, Argos 98) or sigma-dependent rounding in wide-lane followed by ionosphere-free solutions (all other campaigns).

Table 3. Site velocities in ITRF2000, and in a Eurasian reference frame and their formal errors (1-sigma) from TANYA, in mm/yr. The errors have been scaled by the unit variance. The "span" column indicates the interval in months between first and last occupations of the site. v_N, v_E, velocities in north and east direction, $\sigma_N \ \sigma_E$, are the 1-sigma errors in the two directions.

Site	Days	Lat	Lon	Height	v_N ITRF	v_E ITRF	v_N eurasian frame	v_E eurasian frame	σ_N	σ_E	Span
AD18	8	38.32	22.18	131.9	-1.2	5.3	-14.3	-18.9	30.1	30.2	12
AD22	6	38.36	22.24	107	6.0	0.1	-7.0	-24.1	35.4	36.6	12
AETS	2	37.24	21.83	487.4	-19.4	-1.2	-32.5	-25.5	9.4	10.4	21
AGFA	2	37.76	24.91	453.6	-23.2	4.4	-35.9	-20.3	18.9	15.6	25
AGMA	3	38.17	24.07	269.6	-8.4	17.6	-21.2	-6.9	9.4	8.1	25
AGNI	2	37.67	22.49	769.9	-25.6	9.1	-38.6	-15.2	14.5	12.2	13
ANK1	76	39.89	32.76	976.1	9.4	2.5	-2.0	-22.9	2.2	2	37
AR44	8	40.37	21.45	1105.4	9.1	22.0	-4.0	-1.8	2.2	2.1	52
ARIO	3	38.33	21.77	35.8	3.9	30.4	-9.2	6.3	14.6	15.5	21
AS76	5	38.67	22.44	465.1	3.1	9.3	-10.0	-14.9	38.7	38.3	12
ASKT	14	40.93	25.57	182.7	6.3	33.3	-6.2	9.0	3.4	2.9	12
ASTP	4	36.59	26.41	152.3	-13.0	32.6	-25.4	7.5	17.4	17.7	12
ATKO	2	38.49	21.12	163.9	-11.4	32.5	-24.6	8.5	13	10.8	21
AY88	6	39.99	21.74	681.1	0.01	21.5	-13.1	-2.4	2.7	2.5	52
BOR1	96	52.28	17.07	124.4	13.0	21.8	-0.7	1.4	1.9	1.6	63
BRUS	103	50.8	4.36	149.7	15.3	18.4	0.4	0.1	1.7	1.9	75
CAGL	87	39.14	8.97	238.4	14.2	22.5	-0.4	0.4	1.8	2.1	52
CG05	2	39.36	23.19	623.3	-8.9	18.4	-21.8	-5.8	9.4	5.6	24
CG19	5	38.78	22.45	561.6	-4.0	-0.2	-17.0	-24.4	46.9	50.4	12
CG20	4	38.65	22.62	312.3	-1.5	-0.7	-14.5	-25.0	51.1	54.9	12
CG22	6	38.64	22.4	764.1	-5.8	2.1	-18.8	-22.1	49.5	51.4	12
CG30	8	38.4	22.14	890.9	-4.5	10.2	-17.5	-14.0	4.5	4.3	60
CG32	7	38.4	22.58	565	-4.0	0.6	-17.0	-23.6	46.4	43.4	12
CG33	2	38.43	22.87	357.6	-12.8	8.3	-25.7	-16.0	91.4	89.4	12
CG42	5	38.23	21.97	753.9	-17.0	8.8	-30.1	-15.4	9	9.3	39
CG43	7	38.13	22.19	906.3	-13.9	-1.8	-27.0	-26.1	47	48.1	12
CG44	5	38.01	22.64	733.5	-15.9	9.0	-28.9	-15.4	14.2	11.7	25
CG47	4	38.02	22.94	329	-16.7	12.1	-29.7	-12.3	6.1	5.2	24

CG48	2	38.02	23.13	1387.9	-17.1	17.1	-30.0	-7.3	9	7.6	24
CG50	4	38.21	23.35	647.2	-13.8	15.4	-26.7	-9.0	12.1	11.6	49
CG52	2	38.39	23.96	58.6	-17.8	8.3	-30.6	-16.2	22.6	16.9	25
CG53	3	38.23	23.85	499.9	-2.2	17.3	-15.1	-7.1	9.7	9.3	25
CG54	61	38.08	23.93	510.6	-12.7	9.7	-25.6	-14.8	2	2	52
CG55	2	38.35	24.19	181.6	-17.8	8.3	-30.6	-16.2	19.1	17.2	25
CG56	4	38.09	24.39	529.7	-20.1	5.3	-32.8	-19.3	8.4	7.2	33
CG58	3	38.02	23.61	217.5	-11.0	1.7	-23.9	-22.7	10.8	10.5	16
CG61	3	38.01	21.58	287.3	-16.1	3.5	-29.2	-20.7	11.7	13.5	39
CG63	2	37.72	22.88	671.6	-14.8	7.3	-27.8	-17.1	11.5	12.6	49
CG64	2	37.79	22.94	785.2	-19.4	7.8	-32.4	-16.6	21.2	23.1	25
CG65	3	37.8	23.09	426.3	-18.3	7.5	-31.3	-16.9	7.7	6.7	49
CG66	2	37.82	23.94	247.12	-29.1	2.8	-41.9	-21.7	15.8	14.9	25
CJ00	2	37.86	22.74	870.45	-11.7	8.2	-24.7	-16.2	8.7	7.4	25
CK00	2	37.89	22.86	415.8	-6.3	4.0	-19.3	-20.4	7.2	6.5	24
CT00	12	38.38	22.39	61.1	-5.5	15.9	-18.6	-8.3	28.6	28.4	7
DE30	7	39.84	21.88	1323.3	4.3	19.4	-8.9	-4.5	2.5	2.4	52
DION	119	38.08	23.93	514.6	-12.7	7.4	-25.5	-17.1	1.9	1.9	63
DIRO	2	36.64	22.37	105.9	-14.7	1.4	-27.8	-23.1	21.4	18.5	12
DMNA	3	37.71	23.07	245.8	-18.3	9.1	-31.2	-15.4	6.7	5.8	24
DREP	10	38.34	21.85	33.6	-6.1	26.2	-19.3	2.1	5.8	4.8	21
E000	4	38.19	22.1	1018	-9.4	13.7	-22.5	-10.6	6.8	7.2	21
EG62	4	38.13	22.06	1161	-9.4	-5.2	-22.5	-29.4	38.6	44.7	11
EG75	5	38.15	22.14	846.2	-16.8	2.2	-29.9	-22.0	43.1	45.8	11
FORT	71	-3.88	321.57	19.5	6.2	-20.8	-7.2	-45.8	4	6.2	45
G000	5	38.07	21.95	786.9	-3.9	5.7	-17.0	-18.5	6.2	5.6	48
G104	6	40.16	21.36	1028.3	8.7	21.3	-4.5	-2.5	2.5	2.3	52
GOPE	83	49.91	14.79	592.6	13.0	21.4	-1.0	0.8	1.9	1.7	52
GR49	6	40.13	21.29	1071.9	8.7	21.8	-4.5	-2.0	2.4	2.2	52
GR69	8	40.18	21.5	755.6	8.8	18.8	-4.4	-5.0	2.6	2.3	52
GRAZ	92	47.07	15.49	538.3	13.9	21.9	-0.04	0.5	1.8	1.7	72
H000	3	38.53	21.98	599.5	1.8	8.8	-11.3	-15.4	9.2	8.3	21
HERS	104	50.87	0.34	76.5	18.1	27.7	3.0	10.2	1.7	2	63
HFLK	80	47.31	11.39	2384.1	14.6	21.3	0.3	0.7	1.8	1.8	64
HIOS	8	38.44	26.09	647.6	-7.0	3.3	-19.5	-21.5	15.3	12.3	12
I000	4	38.44	21.9	553.2	0.7	13.7	-12.4	-10.4	11.6	8.7	21
IERI	2	40.44	23.85	127	8.1	-1.1	-4.8	-25.2	24.5	18.8	12
ILOK	3	37.44	23.3	328.4	-16.9	6.2	-29.8	-18.3	5.6	5.4	24
IT01	6	38.34	22.29	163.6	-3.6	9.2	-16.7	-15.1	34.8	35.1	12
IT23	6	38.41	22.3	823.6	-7.0	3.1	-20.0	-21.1	37.1	38.4	12
IT61	5	38.49	22.39	533.3	-9.1	-4.6	-22.1	-28.9	44.1	40.7	8

JOZE	92	52.1	21.03	141.5	11.6	21.6	-1.6	0.4	2	1.5	63
K000	2	38.26	21.89	1079.8	-10.7	13.7	-23.8	-10.5	10.4	8.8	20
KALI	3	40.85	22.17	240.6	21.2	21.4	8.1	-2.4	17.6	16.1	24
KATV	7	35.95	27.78	73.9	-17.4	13.1	-29.6	-12.2	9.5	9.6	12
KIT3	47	39.13	66.89	622.5	10.0	21.9	6.3	-6.5	3.2	3.6	48
KIVE	2	37.52	22.69	223.4	-19.5	8.5	-32.5	-15.9	19	17.7	13
KLKI	2	41.01	22.83	385	11.7	9.5	-1.3	-14.3	25.6	24.3	12
KLTH	3	36.89	21.8	295	-23.2	-0.4	-36.3	-24.8	17.4	10.8	21
KN03	9	40.01	21.63	765.7	0.6	19.9	-12.6	-4.0	2.4	2.2	52
KN43	5	40.11	21.62	731.7	5.2	21.5	-7.9	-2.3	2.7	2.5	52
KN49	5	40.14	21.65	956.4	6.6	19.5	-6.5	-4.4	2.3	2.2	52
KN88	8	40.21	21.59	1005.9	9.6	20.2	-3.6	-3.6	2.6	2.4	52
KOIL	3	37.41	23.11	89.6	-14.6	7.8	-27.6	-16.7	7.9	6.7	24
KOSG	154	52.18	5.81	96.9	16.3	18.7	1.5	0.5	1.7	1.8	72
KOSM	2	37.09	22.74	1242.7	-12.3	9.1	-25.3	-15.4	8.7	7.1	24
KRKR	5	38.15	23.7	1200.2	-23.7	2.5	-36.5	-21.9	16.2	24.7	23
KRNA	6	39.94	22.54	984.7	-0.3	24.9	-13.4	0.9	4.7	4	21
KYLN	3	37.94	21.14	48.1	-2.0	36.5	-15.2	12.3	20.4	17	21
KYRA	4	36.31	22.98	297.9	-9.2	12.3	-22.2	-12.3	8.6	9	24
L000	2	38.1	21.81	588.8	-22.4	19.5	-35.6	-4.7	9.7	12.4	20
LAGA	2	40.85	23.54	613.3	5.4	5.7	-7.5	-18.3	25.3	19.7	12
LAMA	87	53.89	20.67	187	12.0	21.3	-1.3	0.7	2.1	1.5	60
LEON	5	37.18	22.82	945.1	-16.4	2.8	-29.4	-21.7	6.8	6.6	21
LEPE	2	38.7	21.29	167.6	1.8	30.4	-11.4	6.4	12.9	10.7	21
LESV	5	39.23	26.45	50.4	-11.4	6.3	-23.8	-18.4	6.7	5.4	12
LEVK	2	38.61	22.2	683.6	-4.0	15.7	-17.1	-8.5	10	8.8	21
LGRN	2	37.68	24	125	-7.4	27.2	-20.2	2.6	16.8	14.4	12
LI29	6	40.06	21.94	1092	3.4	19.7	-9.7	-4.2	2.6	2.4	52
LI74	5	40.21	21.9	415.8	4.5	21.1	-8.6	-2.8	2.6	2.4	52
LIMN	5	39.85	25.13	45.3	-3.3	8.0	-16.0	-16.4	9.1	7.1	12
LIPO	5	39.68	21.85	804.7	2.7	18.4	-10.5	-5.6	3.4	3	25
LO79	6	40.19	22.04	898.4	4.3	20.1	-8.8	-3.8	2.8	3.5	52
LTSA	2	37.95	24	253.3	-15.3	6.5	-28.1	-18.0	20.9	17.7	12
MADR	92	40.43	355.75	829.5	15.9	18.4	0.6	-1.1	1.8	2.3	72
MAOR	3	38.19	21.39	73.4	-11.9	28.1	-25.0	4.0	12.2	9.4	21
MAS1	73	27.76	344.37	197.2	16.2	17.7	1.0	-3.3	2.2	3.1	49
MATE	115	40.65	16.7	535.7	17.1	23.4	3.4	0.4	1.8	1.9	72
MDVO	66	56.03	37.22	254.8	13.2	22.2	2.7	-0.7	2.5	1.6	52
MEDI	81	44.52	11.65	50.1	15.9	23.8	1.6	2.5	1.8	1.8	52
MESS	2	38.37	21.12	26.5	-4.1	27.1	-17.3	3.1	13.7	11.4	22
METS	73	60.22	24.4	94.6	9.0	22.4	-3.8	2.9	2.3	1.5	69

MLDR	2	37.75	22.64	511.7	-4.7	16.2	-17.7	-8.2	19	15.6	12
MLSS	2	37.95	21.35	119.5	-12.2	22.5	-25.4	-1.7	14	12.4	21
MLVN	2	37.17	22.25	1641.7	-16.8	4.2	-29.9	-20.2	16.3	18.2	21
MNVS	4	36.74	23.08	136.1	-20.6	5.3	-33.5	-19.2	11	9.4	21
MYRT	2	38.07	21.5	153.9	-14.2	12.7	-27.4	-11.5	25.5	23.9	9
NEVR	3	41.35	23.85	956	4.1	-10.2	-8.8	-34.2	9.9	9	24
NICO	54	35.14	33.4	190	15.4	16.8	4.2	-9.2	2.2	2.3	36
NOTO	135	36.88	14.99	126.2	16.6	18.2	2.6	-5.2	1.8	2	60
ONSA	144	57.4	11.93	45.6	12.9	19.8	-1.4	1.9	1.9	1.7	72
OREI	3	37.35	22.66	865.4	-13.0	14.6	-26.0	-9.8	14.5	14.1	24
OXIA	4	39.76	21.94	1447.8	8.8	18.5	-4.3	-5.5	10.6	9.2	9
P842	2	40.6	21.68	808.9	3.7	19.7	-9.4	-4.1	3.9	3.2	36
PENC	80	47.79	19.28	291.8	12.7	22.8	-0.7	0.9	1.9	1.6	52
PHEL	2	37.3	23.17	96.3	-19.7	10.6	-32.6	-13.9	15.5	14.4	11
PIGA	2	37.07	22.91	755.6	-25.2	14.7	-38.2	-9.8	14.4	13.3	11
PLAT	2	40.64	23.36	561.9	1.3	0.5	-11.6	-23.5	22.1	18.6	12
PLNI	4	37.18	22.13	999.5	-8.1	2.7	-21.2	-21.7	11.8	11.1	21
POTS	95	52.38	13.07	144.4	13.2	19.9	-1.0	0.3	1.9	1.7	63
PRST	4	36.88	22.24	198.3	-12.9	3.8	-26.0	-20.6	15.6	12.8	21
PSMS	9	40.37	23.44	614.7	0.1	-10.1	-12.8	-34.2	4.4	3.6	24
PYLO	3	36.89	21.7	507.9	-23.9	5.4	-37.0	-19.0	17.4	9.5	21
RASK	2	37.98	23.31	262.4	-2.3	24.2	-15.2	-0.2	10	8.8	24
RIOE	2	38.31	21.78	35.5	0.0	11.2	-13.2	-13.0	24.8	57.1	9
RION	2	38.31	21.78	34.2	-3.6	10.4	-16.7	-13.8	18.5	15.6	12
ROML	7	35.4	24.69	102.4	-20.1	13.5	-32.8	-11.5	6.1	5.5	12
SANT	50	-33.15	289.33	723	21.2	39.1	13.9	11.2	5.9	9.8	24
SFER	83	36.46	353.79	84.2	17.0	16.5	1.7	-3.7	1.9	2.5	52
SI19	6	40.3	21.7	743.5	6.4	19.8	-6.8	-4.0	2.7	2.4	52
SI34	8	40.34	21.56	1070.5	7.8	22.6	-5.4	-1.2	2.5	2.3	52
SI80	6	40.47	21.51	1636.7	7.7	21.2	-5.5	-2.6	2.3	2.2	52
SIFB	8	40.24	21.57	807.7	15.2	19.1	2.0	-4.7	4.3	4	27
SOFI	50	42.56	23.39	1119.6	10.4	23.4	-2.5	-0.2	2	1.8	36
STHN	6	39.99	23.92	158.8	-0.1	12.6	-12.9	-11.6	2.7	2.4	36
STRF	2	37.07	21.87	285.5	-18.9	-6.4	-32.0	-30.7	25.8	29.2	21
STRV	3	37.1	22.41	375.6	-33.3	0.4	-46.4	-24.1	32.2	25.3	9
THEO	2	40.96	23.12	786.2	13.0	-0.2	0.02	-24.1	24.3	27.5	12
THIR	4	36.35	25.44	197	-10.6	17.7	-23.2	-7.3	10.1	13.1	12
THOM	3	38.39	21.49	152.9	-16.5	8.2	-29.7	-15.9	18.8	17.8	9
TOLO	3	38.32	22.18	131.9	-1.9	17.0	-14.9	-7.2	12.3	11.2	21
TSUK	3	40.86	21.88	1123.3	7.9	11.7	-5.2	-12.1	4.8	4.3	36
TZIA	2	37.62	24.37	564.6	-24.6	3.7	-37.3	-20.9	15.3	15.8	24

UPAD	75	45.41	11.88	84	16.3	21.8	2.0	0.7	1.8	1.8	52
VELI	7	36.72	22.95	248.1	-21.7	7.1	-34.7	-17.5	6.3	6.2	21
VILL	103	40.44	356.05	647.4	15.2	22.1	-0.1	2.5	1.8	2.3	63
VRES	2	40.8	23.14	458	9.5	6.3	-3.5	-17.6	15.9	15.7	12
VRMS	2	37.46	23.47	574.1	-18.3	2.6	-31.2	-22.0	15.6	13.9	12
WARE	52	50.69	5.25	187.9	15.9	18.0	1.0	-0.5	1.9	1.9	28
WTZR	98	49.14	12.88	666	13.5	20.9	-0.7	0.5	1.8	1.7	52
XRIS	9	36.79	21.88	476.3	-18.2	6.4	-31.3	-18.0	2.6	2.8	45
YITH	2	36.78	22.56	149.1	-21.5	14.9	-34.5	-9.6	16.1	15	12
ZIMM	103	46.88	7.47	956.3	15.1	20.1	0.5	0.1	1.7	1.9	72
ZWEN	67	55.7	36.76	205	9.0	23.9	-1.7	1.0	2.5	1.6	63

Table 4. Principal horizontal strain rates (Eps1 and Eps2), azimuth of most compressive principal strain, and rates of rotation and dilatation.

Polygon	Eps1 (ppm/yr)	1σ	Eps2 (ppm/yr)	1σ	Azim (degrees)	1σ	Rotation (degMyr)	1σ	Dilatation (ppm/yr)	1σ	Goodness of fit (χ^2)	Number of sites
1	0.28	0.16	-0.05	0.15	-72.5	35.1	11.1	6.0	0.23	0.22	1.97	7
2	0.04	0.10	0.03	0.13	-75.8	50.7	1.5	5.0	0.06	0.16	3.25	13
3	0.05	0.23	-0.08	0.15	-54.2	50.7	10.1	7.8	-0.03	0.26	0.45	5
4	0.04	0.23	0.01	0.18	-7.6	50.7	-8.2	9.4	0.04	0.29	1.33	9
5	0.10	0.20	-0.16	0.48	88.2	47.7	2.3	17.6	-0.06	0.52	1.10	6
6	0.09	0.05	-0.13	0.08	79.2	21.3	-0.5	2.9	-0.04	0.10	0.43	4
7	0.19	0.13	-0.24	0.11	-89.6	16.3	0.7	5.0	-0.04	0.17	6.13	14
8	0.24	0.22	0.01	0.61	79.0	49.3	3.3	19.0	0.25	0.65	0.30	10
9	0.04	0.51	-0.13	1.91	-28.6	50.8	11.2	56.8	-0.09	1.99	0.48	6
10	0.11	0.40	0.01	0.20	-15.0	50.2	7.7	12.3	0.12	0.44	0.02	5
11	0.10	0.10	0.01	0.12	-32.7	50.6	2.0	4.6	0.11	0.16	8.39	16
12	0.15	0.18	-0.17	0.14	74.0	35.3	3.6	6.4	-0.02	0.23	10.10	12
13	0.03	0.07	-0.04	0.06	57.0	50.5	3.0	2.9	0.00	0.08	2.66	5
14	0.08	0.05	-0.05	0.03	-75.1	26.5	1.6	1.7	0.03	0.06	0.48	8
15	0.09	0.11	0.00	0.06	-71.5	47.4	-3.0	3.4	0.09	0.13	0.02	4
16	0.01	0.05	-0.18	0.19	31.0	50.1	-2.2	6.1	-0.17	0.20	0.11	4
17	0.09	0.10	0.01	0.04	-43.6	50.8	-1.3	2.9	0.10	0.11	0.10	5
18	0.10	0.12	-0.02	0.07	-80.3	43.3	1.7	4.7	0.09	0.14	0.00	3
19	0.15	0.36	-0.30	0.27	12.4	41.0	-0.5	13.9	-0.15	0.44	0.00	3
20	0.07	0.02	-0.05	0.03	63.5	34.6	2.1	1.2	0.02	0.04	24.30	22
21	0.11	0.07	-0.06	0.04	76.8	23.4	-2.1	1.9	0.05	0.08	1.10	9
22	0.20	0.06	0.02	0.03	-38.0	50.4	6.1	2.0	0.21	0.07	0.40	7

Table 5. Seismic strain rates in ppm/yr for the three seismic catalogues and a 15 km thickness of the seismogenic layer. Note that not all polygons are covered by every catalogue.

a) 30-year catalogue							
Polygon	**Shear 1 (γ_1)**	**Shear 2 (γ_2)**	**Dilatation (Δ)**	**Total shear (Γ)**	**Eps1**	**Eps2**	**Azim2 (deg)**
1	-0.0014	-0.0001	0.0013	0.0014	0.0014	0.0000	87.1
2	0.0056	-0.0040	0.0043	0.0068	0.0056	-0.0013	17.9
4	-0.0002	0.0035	0.0043	0.0035	0.0039	0.0004	-46.4
5	-0.0059	0.0028	0.0032	0.0065	0.0049	-0.0017	-77.1
6	-0.0004	-0.0002	0.0004	0.0004	0.0004	0.0000	77.0
7	-0.0056	0.0018	0.0023	0.0059	0.0041	-0.0018	-81.0
8	-0.0678	0.0108	0.0663	0.0687	0.0675	-0.0012	-85.5
9	-0.2379	-0.0773	0.1738	0.2501	0.2120	-0.0382	81.0
10	-0.0043	0.0005	0.0026	0.0043	0.0034	-0.0009	-86.5
11	-0.0654	-0.0312	0.0664	0.0724	0.0694	-0.0030	77.2
12	-0.0081	0.0069	0.0105	0.0107	0.0106	-0.0001	-69.8
14	-0.0649	0.0002	-0.0018	0.0649	0.0316	-0.0333	-89.9
15	-0.0009	0.0002	0.0006	0.0009	0.0007	-0.0001	-83.2
16	0.0000	-0.0001	0.0001	0.0001	0.0001	0.0000	35.6
17	-0.0009	0.0003	0.0008	0.0010	0.0009	-0.0001	-80.3
18	0.0049	-0.0057	0.0069	0.0075	0.0072	-0.0003	24.8
20	-0.0203	-0.0221	0.0296	0.0300	0.0298	-0.0002	66.3
21	-0.0392	0.0107	0.0019	0.0407	0.0213	-0.0194	-82.4
22	-0.0001	0.0001	0.0001	0.0002	0.0002	0.0000	-70.0

b) 100-year catalogue							
Polygon	**Shear 1 (γ_1)**	**Shear 2 (γ_2)**	**Dilatation (Δ)**	**Total shear (Γ)**	**Eps1**	**Eps2**	**Azim2 (deg)**
3	-0.0050	0.0000	0.0020	0.0050	0.0035	-0.0015	89.9
6	0.0098	0.0063	0.0098	0.0117	0.0108	-0.0009	-16.3
7	0.0112	0.0011	0.0066	0.0113	0.0089	-0.0023	-2.9
8	-0.0017	0.0261	0.0017	0.0261	0.0139	-0.0122	-46.9
10	-0.0178	0.0110	0.0177	0.0209	0.0193	-0.0016	-74.2
11	-0.0467	-0.0059	0.0427	0.0471	0.0449	-0.0022	86.4
12	-0.0408	0.0000	0.0432	0.0408	0.0420	0.0012	90.0
13	-0.0028	0.0203	0.0028	0.0205	0.0117	-0.0089	-48.9
14	-0.0240	0.0041	0.0345	0.0244	0.0294	0.0051	-85.1
16	-0.0120	-0.0277	0.0042	0.0302	0.0172	-0.0130	56.7
17	-0.0160	0.0034	0.0320	0.0163	0.0242	0.0078	-84.0
20	0.0040	0.0020	0.0053	0.0045	0.0049	0.0004	-13.0

21	0.0002	0.0019	0.0026	0.0019	0.0023	0.0004	-41.4

c) 300-year catalogue

Polygon	Shear 1 (γ_1)	Shear 2 (γ_2)	Dilatation (Δ)	Total shear (Γ)	Eps1	Eps2	Azim2 (deg)
7	-0.0314	0.0000	0.0314	0.0314	0.0314	0.0000	90.0
8	-0.0428	0.0067	0.0348	0.0433	0.0391	-0.0043	-85.6
9	-0.0195	0.0277	0.0195	0.0339	0.0267	-0.0072	-62.6
10	-0.0152	0.0034	0.0138	0.0156	0.0147	-0.0009	-83.6
11	-0.0218	0.0004	0.0233	0.0218	0.0226	0.0007	-89.4